Journal of Energy Storage 78 (2024) 110110

Contents lists available at ScienceDirect

Journal of Energy Storage

journal homepage: www.elsevier.com/locate/est

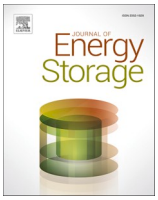

Research Papers

Thermally enhanced nanocomposite phase change material slurry for solar-thermal energy storage

Oguzhan Kazaz [a], Nader Karimi [a,b], Shanmugam Kumar [a], Gioia Falcone [a], Manosh C. Paul [a,*]

[a] Systems, Power & Energy Research Division, James Watt School of Engineering, University of Glasgow, Glasgow G12 8QQ, UK
[b] School of Engineering and Materials Science, Queen Mary University of London, London E1 4NS, UK

ARTICLE INFO

Keywords:
Latent heat thermal energy storage
Phase change slurry
Nano encapsulated PCMs
Heat transfer enhancement
Phase change material
Photothermal conversion and storage

ABSTRACT

This paper investigates the photothermal conversion performance of an innovative heat transfer fluid containing nano-encapsulated phase change material (PCM) with metallic shell materials in a solar thermal energy storage system. The influences of shell thickness, core size, shell material type, PCM mass and shell volume concentrations on the thermal performance of the heat storage medium are investigated and compared. The results show that the heat transfer rates of water-based Ag, Au, Cu and Al nanofluids are 6.89, 5.86, 7.05 and 6.99 W, respectively, while slurries formed by adding paraffin@Ag, Au, Cu and Al nano capsules to pure water enhance heat transfer by 6.18, 13.38, 10.8 and 11.33 %, respectively. The metallic nanoparticle-based shell materials further augment the temperature and energy storage gains by enhancing the solar radiation capture capability of the heat storage medium. Specifically, depending on the mass concentration of PCM, the storage capacity of paraffin@Cu slurry is augmented by up to 290 %. As the shell thickness of the Ag particles also decreases from 8 to 2 nm, it augments the slurry's storage ability for thermal energy by 7 %. The enhancement in the dimensions of the nano capsules, however, causes the surface area-to-volume ratio (*SA:V*) to reduce the photothermal conversion of the slurry by clustering. Therefore, the thermal energy storage behaviour of the Paraffin@Cu slurry is diminished by 5 % as the core size enhances from 10 to 40 nm. Further, the augmentation in the volume concentration of Al particles in the shell surprisingly reduces the thermal energy storage by 5 %. Finally, paraffin-based solid PCM is also experimentally tested for validation of the specific heat capacity model at various wind speeds and solar radiation.

1. Introduction

Increased utilisation of solar energy, which is one of the renewable energy sources, as a heat/energy source can help reduce carbon emissions and prevent global temperature rise [1]. Due to the interruption of natural source-based solar rays, it causes the supply and demand balance in solar energy to be impeded. Thermal energy storage techniques, in addition to providing this balance in energy, can prevent this negativity and provide the continuous use of solar energy in an efficient and reliable way. Thermal energy can be stored by latent, sensible, and thermochemical methods. While sensible energy storage depends on the temperature increment in a heat storage material, latent energy storage is based on the phase transformation of storage material. Nevertheless, a thermochemical energy storage technique is based on reversible chemical reactions [2]. Depending on the temperature enhancement of water or nanofluids [3], systems that absorb thermal energy in the form of sensible heat maybe preferred due to their low installation cost, easy installation and working principle [2]. When the heat source that augments the temperature is removed, the diminish in the storage medium's temperature accelerates, preventing the solar energy from being stored effectively for 24 h. In addition, since the sensible heat storage is based on the material's specific heat capacity as well as the temperature increment, the thermal energy may not be stored optimally. These problems encountered in solar energy storage can be overcome by utilizing phase change materials (PCMs), as PCMs with high latent heat capacity improve energy storage by storing this heat during phase transition as their temperature increments. PCMs can also create a cycle by using this high energy they store as they transition from solid to liquid at phase change temperatures as they transition from liquid to solid at night. Thus, by applying solar energy for one day, the supply and demand situation in energy can be balanced [4]. These advantages of PCMs are already used in solar system applications [5,6].

Bejan et al. [7] experimentally compared the transpired opaque solar

* Corresponding author.
E-mail address: Manosh.Paul@glasgow.ac.uk (M.C. Paul).

https://doi.org/10.1016/j.est.2023.110110
Received 4 August 2023; Received in revised form 5 December 2023; Accepted 11 December 2023
Available online 8 January 2024

Nomenclature

$K_{a\lambda}$	Absorption coefficient (1/m)
C_{abs}	Absorption cross sections (cm^2)
Q_{abs}	Absorption efficiency of core/shell
k	Absorption index
L/H	Aspect ratio
$I_{b\lambda}$	Black body intensity ($W/m^2\mu m$)
l_∞	Bulk free electron mean free path
τ_{bulk}	Bulk metal free electron scattering time
w_p	Bulk plasma frequency
h	Convective heat transfer coefficient
ε	Dielectric function
$\vec{s}$	Direction vector
$\varepsilon_\alpha, \varepsilon_b$	Effective dielectric function
R	Effective mean free path
E	Energy gain
$K_{e\lambda}$	Extinction coefficient (1/m)
C_{ext}	Extinction cross sections (cm^2)
V_f	Fermi velocity
U	Fluid velocity (m/s)
A	Geometric parameter
q	Heat (J/kg)
γ_∞	Inverse of the bulk relaxation time
H	Latent heat of fusion (J/kg)
c_m	Mass concentration
$\dot{m}$	Mass flow rate (kg/s)
ε_{bulk}	Metallic shell dielectric function
$MPCS$	Microencapsulated phase change slurry
N_T	Particle number in unit volume
PCM	Phase change material
α	Polarizability
$\vec{r}$	Position vector
p	Pressure (Pa)
I_λ	Radiation intensity ($W/m^2\mu m$)
q_r	Radiative heat flux (W/m^2)
r	Radius
P	Ratio of shell volume to total particle volume
n	Refractive index
σ_s	Scattering coefficient (1/m)
C_{sca}	Scattering cross sections (cm^2)
$\vec{s}'$	Scattering direction vector
Q_{sca}	Scattering efficiency of core/shell
$\gamma(R)$	Scattering rate
f	Shell concentration
C_p	Specific heat (J/kgK)
α_λ	Spectral absorption coefficient (1/m)
$SA:V$	Surface area-to-volume ratio (1/m)
T	Temperature (K)
k	Thermal conductivity (W/mK)
ΔH	Total enthalpy change (J/kg)
u, v	Velocity vectors (m/s)
w	Wind speed (m/s)

Greek symbols

ρ	Density (kg/m^3)
Φ	Dissipation functions
μ	Dynamic viscosity (Ns/m^2)
ϵ	Emissivity
Ω'	Phase function
σ	Stefan-Boltzmann constant (5.67×10^{-8} W/m^2K^4)
λ	Wavelength of incident light (μm)

Subscripts

amb	Ambient
bf	Base fluid
1	Core
in	Inlet
l	Liquidus
3	Outer region
out	Outlet
r	Radiative
2	Shell
s	Solidus

collector's thermal behaviour with and without PCM. Paraffin RT35 was used as an organic PCM. Their findings showed that transpired opaque solar collector with PCM had better thermal capacity. The maximum efficiency and heating capacity were augmented by 6 and 7.7 %, respectively. It was also noticed that the mean heating capacity was 5 times better during the discharging period. The mean performance coefficient was also 16.4 % greater and the PCM supplied over 17 % additional energy as 5900 Wh during its 9-hour runtime. The authors suggested that the PCM based transpired opaque solar collector integrated into buildings could be investigated under actual atmospheric conditions for greater operating time. The thermal capacity of PCM-based solar collector was examined by Feng et al. [8]. Thermal conductivity, PCM's enthalpy and melting points were considered as working parameters. The influences of the flow rate of the fluid and the mass fraction of the Multi-Walled Carbon Nanotubes on the thermal performance were also evaluated. It was observed that the increment in the PCM's melting point negatively affected the performance. The numerical outcomes also showed that the optimum capacity was obtained using a medium enthalpy based PCM. As the PCM's thermal conductivity increased, the higher thermal energy was provided by augmenting the heat transfer rate between the fluid and the absorber plate. The PCM based collector's performance was augmented by improving the fluid's flow rate and Multi-Walled Carbon Nanotubes fraction.

Comparative examination of a conventional flat plate solar collector with and without PCM under real surrounding operations was experimentally and mathematically conducted by Palacio et al. [9]. Solar irradiation, wind velocity, water outlet and inlet temperatures, atmospheric temperature and temperatures of the absorber wall, glass plate and PCM were monitored during experiment. A mathematical technique was used for estimating the PCM's melt fraction and heat losses. Two dissimilar PCMs were employed, having melting points at 60 °C (PCM-1) and 41 °C (PCM-2) respectively. The results showed that although PCM-1 had a better density, melting point, and fusion heat, PCM-2 contributed to a higher thermal energy thus a melt fraction. The PCM type and contact conduction between the PCM and absorber were discovered as the main elements of performance enhancement. The collector with PCM enhanced the night output temperature by 2 °C and subsequently, the highest collected energy by 630 Wh.

However, PCMs have a low thermal conductivity and can cause leakage during phase transformations. Hence, an additional storage unit is preferred as it cannot interact with pure fluids. Encapsulation techniques can be used to protect the PCMs' shape by enclosing them with a shell and to prevent leakage [10,11]. An improved heat storage material, therefore, can be obtained by improving both the optical and thermophysical properties of an encapsulated PCM. Thanks to these augmented properties, new types of encapsulated PCM slurries or latent functionally thermal fluids can be prepared by dispersing them into pure heat transfer fluids [12,13] and used in solar energy applications [14,15]. Eisapour et al. [16] numerically analysed the photovoltaic-thermal performance with wavy tubes in a water-cooled photovoltaic-

thermal system. The performances of wavy and straight tubes were compared for different wave amplitudes and wavelengths. Ag/water nanofluid, water, microencapsulated PCM nano-slurry, and microencapsulated PCM slurry were applied as coolant fluids. The findings demonstrated that the photovoltaic-thermal module with wavy tubes had better electrical, exergy and thermal efficiencies. The heat absorption of the working fluid was enhanced by diminishing the wavelength in a constant amplitude/wavelength. It was also displayed that the microencapsulated PCM nano-slurry had better thermal behaviour due to having higher heat capacity and thermal conductivity. The exergy and primary efficiencies of the system augmented by 4.25 and 6.06 %, respectively, for the wavy tube compared to a straight tube system.

Jia et al. [17] assessed the microencapsulated phase change slurry's (MPCS) performance in a photovoltaic-thermal system. The impressions of channel height, mass fraction and flow rate on the electrical and thermal performances were considered as working conditions. The numerical results indicated that the thermal efficiency was altered by ambient temperature and solar irradiation density. The solar radiation power also impacted the electrical performance, and it was discovered that the electrical and thermal capabilities of the photovoltaic-thermal system were augmented by the temperature of photovoltaic panel and heat transfer fluid as MPCS had a lower temperature increment compared to pure water. The overall thermal performance was obtained using MPCS at a mass fraction of 15 %. It was then uncovered that as the mass fraction improved, the temperature drop of the photovoltaic panel decreased. Qiu et al. [18] applied a mathematical model to further analyse the MPCS-based PV/T module's energy performance using various operating conditions such as concentration ratio, slurry flow state and serpentine size, and Reynolds number. It was unearthed that the PV/T system's performance was enhanced by using MPCS. The outcomes also revealed that as the serpentine piping diameter enhanced, the slurry's flow rate improved, reducing the PV cells' temperature, thereby augmenting the module's electrical, net, thermal, and overall efficiency. Moreover, it was observed that increasing the microencapsulated PCM concentration ratio at a given flow rate did not affect the heat transfer and PV/T's performance.

The absorbing medium of solar systems, where the fluid is directly heated by the solar light, functions as a heat transfer fluid, while it can also be employed as a heat storage medium. Therefore, due to the high latent heat capacity of an encapsulated PCM slurry, it can be utilized as a working fluid to augment the system efficiency [19,20]. In this context, Liu et al. [21] carried out an experimental scrutiny to analyse the microencapsulated PCM slurry's photothermal conversion performance. The GO-CNT hybrid filler's effect on the thermal and morphology behaviours of the microcapsules was also analysed. Dodecanol core and melamine-formaldehyde (MF) resin were used as PCM and shell materials, respectively. They also modified the shell material using a carbon nanotube (CNT) hybrid filler and Graphene oxide (GO). Their results showed that the impact of GO and CNT materials on a spherical capsule was meagre. It was also discovered that the microencapsulated PCM's thermal conductivity was improved by 195 % with a GO-CNT hybrid filler. Therefore, slurry could be a favourable heat transfer fluid in solar applications due to the high optical properties and thermal conductivity. Paraffin@TiO_2 and paraffin@TiO_2/GO composite microcapsules were prepared by *Ma* et al. [22] for thermal energy storage applications. Their experiment unearthed that the paraffin@TiO_2/GO composite exhibited better thermal balance than paraffin due to the shell material. The new slurry was formed by dispersing the paraffin@TiO_2/GO composite into pure water. Since the paraffin had phase change process, the paraffin@TiO_2/GO and paraffin@TiO_2 slurries had better specific heat capacities compared to pure water. The paraffin@TiO_2/GO slurry had an impressive photothermal conversion capability due to its higher thermal conductivity and optical absorption than that of paraffin@TiO_2 composite. It was suggested that the new slurry including paraffin@TiO_2/GO microcapsules could be beneficial for augmenting the collector efficiency. Xu et al. [23] conducted experimental research on paraffin@Cu-Cu_2O/CNTs, where paraffin was a core material and Cu, Cu_2O and CNTs (carbon nanotubes) as shell materials. Paraffin@Cu-Cu_2O/CNTs microcapsules were also shown to enhance the thermal decomposition temperature by approximately 50 °C compared to the paraffin@Cu-Cu_2O microcapsule with higher thermal stability. Furthermore, it was recognised that the paraffin@Cu-Cu2O/CNTs based slurry due to its superior absorption, thermal conductivity and specific heat characteristics provided better photothermal conversion performance.

Microencapsulated PCMs addition to the base fluid enhances the thermal capacity of the system as seen in previous examples. Microcapsules, on the other hand, can easily be broken and increase the fluid's viscosity during the fluid flow process. This issue affects the long-term pump or fluid circulation which limits the application of microcapsules. Since nano-encapsulated PCMs have low breakage during pumping, small particle diameter, suspension stability and large surface area compared to microencapsulated PCMs, they are preferred in the application of thermal management and energy storage [24]. Spray-drying, radical addition-fragmentation chain-transfer, layer-by-layer assembly, creation of dendrimers, precipitation of pre-formed polymers, mini-emulsion polymerisation are also techniques to create the nano-encapsulated PCMs [25].

The application of organic shell materials has restrictions during the capsulation of PCMs due to the insufficient mechanical properties, low thermal conductivity, and flammability [26]. In order to prevent this negativity, the materials that have higher thermal conductivity, better mechanical strength, and higher rigidity can be used as shell materials. Zhou et al. [27] prepared a copper (Cu)-based capsule with Al shell material for thermal energy storage applications. The Al shell was filled with Cu beads, the Cu—Al atomized powder was filled in the gap, and then it was heat treated. The experimental results showed that the corrosion of copper oxide (CuO) on the Al shell was diminished by mixing Al with Cu. The area around the hole contributed at the top of the spherical shell gets sealed, thereby suppressing the flow of oxygen into the shell owing to this two-step reaction. The alloy in copper-rich areas was found to show relative stability in thermal properties and distribution during subsequent cycles. While the capsule's slight damage load change after the exposure showed good mechanical stability, a low weight increase ratio of 3.5 % after the exposure revealed the capsule's good oxidation resistance. A facile paraffin sacrificial layer approach for directly encapsulating Cu sphere PCMs with the Al_2O_3 shell which considers the buffer inner cavity was developed by Zhao et al. [28] in the field of long-term thermal energy storage. The cavity was built by the paraffin layer's decomposition through a pre-sintered process. It provided a significant role in accommodating the core's volume expansion, thereby preventing the shell's breakage and the liquid PCM's leakage. The experimental results revealed that the Al_2O_3 shell possessed a good structure that prevented the leakage of the Cu core. The Al_2O_3 shell also had strong compatibility with the Cu core without any chemical reaction between two materials. The capsule's mass and volume energy storage densities were 1.83 and 1.76 times, respectively, better than those for the Al_2O_3.

1.1. Contribution of this paper

PCMs and encapsulated PCM slurries have been used in solar system applications, however, there are important research gaps identified through the literature review above, regarding the use of nano-encapsulated PCM slurry as an energy storage medium in those systems. The novelties in this study, thus, can be listed as follows:

- For the first-time, the paper investigates the photothermal transformation of a directly heated solar system filled with a slurry obtained by nano-encapsulated PCM with metallic shell materials dispersed in pure water, under various flow conditions. Nano-encapsulation is preferred in this study due to its advantages such as

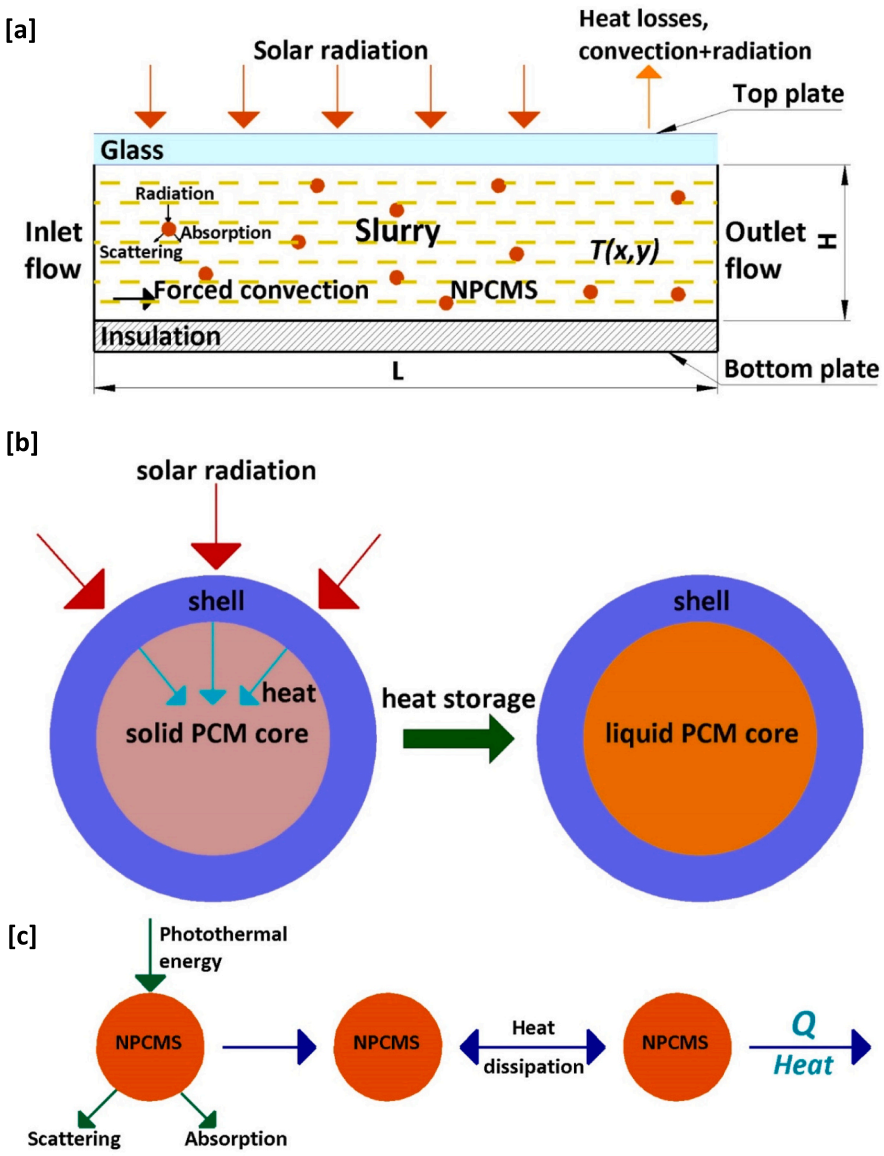

Fig. 1. (a) The schematic of the nanoencapsulated PCM slurry based directly heated solar system, (b) effect of radiation on nanoencapsulated PCM, and (c) effect of radiation on a nano capsule within the slurry.

enhancing the heat transfer capacity of PCM by improving its thermal conductivity, maintaining its stability, and preventing leakage in the phase transformation.

- The influences of PCM, base fluid and shell material types, which are the structures that make up nano-encapsulated PCM slurry, on the heat storage medium's optical and thermophysical behaviours are investigated. Since different types of shell materials have dissimilar features that directly affect the system performance, the impacts of them needs to be analysed and compared under the semi-transparent flow conditions. It also examines the metallic shell's effect on nano capsules due to the surface plasmon resonance effect in the heat storage medium under solar radiation.
- Besides, the change in particle size alters the particle distribution in the base fluid, thus affecting its capacity to capture solar energy. Because of this reason, the influences of shell thickness and PCM size on the system performance are still lacking in the literature. Since the mass concentration of a PCM has a direct impact on photothermal conversion, there is a need to investigate at what level its impact occurs. How does the continuous augmentation of the concentration amount modify the temperature gain of the heat transfer fluid? How does this enhancement in temperature alter the thermal energy storage? Furthermore, the thermal performance behaviour of nano-encapsulated PCM slurry under combined forced convection and radiation heat transfer is still unknown and this paper fills that research gap too. The effect of the volumetrically heated heat transfer fluid on the PCM capsules under this combined effect is also a matter of curiosity because the factors explained above may alter the nano capsules and change the fluid's heat transfer behaviour.

Taking all these into consideration, the inspiration of the current research is to contribute to the literature by filling these knowledge gaps regarding the solar-to-thermal heat conversion and storage by conducting a comprehensive study. Moreover, in the experimental study, thermal behaviour of pure PCM was examined under different wind speeds and solar heat fluxes considering the relevant environmental factors and it was illustrated that it can be used as an alternative to the enthalpy method by validating the experimental data by implementing the specific heat capacity model.

Table 1
Bulk mean free path, bulk plasma frequency and fermi velocity of shell materials [44].

	Cu	*Al*	Ag	Au
Fermi velocity (10^6 m/s)	1.57	2.03	1.39	1.38
Bulk mean free path (nm)	42	16	52	42
Bulk plasma frequency (10^{16} Hz)	1.64	2.4	1.36	1.37

2. Problem statement and mathematical formulation

A two-dimensional heat transfer and fluid flow model is established and numerically solved to analyse the photothermal conversion behaviour of a nano-encapsulated PCM slurry based directly heated solar system having the aspect ratio (*L/H)* of 10 [29] as exhibited in Fig. 1(a). The collector's top plate is covered with a transparent glass surface to enable most of the sunlight to pass, thus facilitating the penetration of sun's rays into the collector [1]. Radiation coupled with convection heat loss to the atmosphere also occurs from this transparent surface [30]. Furthermore, the nanoencapsulated PCM consists of the shell and core (Fig. 1(b)). The solid PCM's temperature, which is surrounded by the shell structure, increases with the radiation, and approaches the melting temperature. Thus, the liquid PCM is obtained. Protected by the shell, the PCM hampers the leaking during phase transformation, suspending it from blending with the host fluid. Moreover, when the sunbeam performs on uniformly dispersed nano capsules in the host fluid, as seen in Fig. 1(c), they start to capture the solar energy due to the metallic shell's optical properties [31]. Thus, the nano capsules reacting to by colliding with each other both improve the temperature of the slurry because of heat transfer and augment the heat storage of the slurry during the PCM's phase transformation.

The Equation of Radiative Transfer is implemented to calculate the irradiation's spectral attenuation within the semi-transparent flow condition, and is identified as [32]:

$$\nabla \bullet (I_\lambda(\vec{r},\vec{s})\vec{s}) + (\alpha_\lambda+\sigma_s)I_\lambda(\vec{r},\vec{s}) = \alpha_\lambda n^2 I_{b\lambda} + \frac{\sigma_s}{4\pi}\int_0^{4\pi} I_\lambda(\vec{r},\vec{s}')\Phi(\vec{s}\bullet\vec{s}')d\Omega' \quad (1)$$

The scattering effects can be neglected in pure fluids (water) as absorption attenuation dominates. Thus, the extinction coefficient is described as [33]:

$$K_{e\lambda,bf} = K_{a\lambda,bf} = \frac{4\pi k}{\lambda} \quad (2)$$

The dipole model can explain the core-shell capsules' absorption and scattering efficiencies as [34,35]:

$$Q_{abs} = C_{abs}/(\pi a^2) = kIm(\alpha)/(\pi a^2) = \frac{8\pi^2\sqrt{\epsilon_3}}{\lambda} r_2^3 Im\left(\frac{\varepsilon_2\varepsilon_\alpha - \varepsilon_3\varepsilon_b}{\varepsilon_2\varepsilon_\alpha + 2\varepsilon_3\varepsilon_b}\right)/(\pi a^2) \quad (3)$$

and

$$Q_{sca} = C_{sca}/(\pi a^2) = \frac{k^4}{6\pi}|\alpha|^2/(\pi a^2) = \frac{128\pi^5}{3\lambda^4}\varepsilon_3^2 r_2^6\left|\frac{\varepsilon_2\varepsilon_\alpha - \varepsilon_3\varepsilon_b}{\varepsilon_2\varepsilon_\alpha + 2\varepsilon_3\varepsilon_b}\right|^2/(\pi a^2) \quad (4)$$

where $k = 2\pi n/\lambda$, and α can be determined as [36]:

$$\alpha = 4\pi r_2^3[(\varepsilon_2\varepsilon_\alpha - \varepsilon_3\varepsilon_b)/(\varepsilon_2\varepsilon_\alpha + 2\varepsilon_3\varepsilon_b)] \quad (5)$$

where:

$$\varepsilon_b = \varepsilon_1 P + \varepsilon_2(3-P) \quad (6)$$

$$\varepsilon_\alpha = \varepsilon_1(3-2P) + 2\varepsilon_2 P \quad (7)$$

$$P = 1 - (r_1/r_2)^3 \quad (8)$$

The core-shell capsule's extinction coefficient is calculated as [37]:

$$K_{e\lambda} = C_{ext}N_T = \left(\pi a^2(Q_{abs}+Q_{sca})\right)\left(6f/\pi D^3\right) \quad (9)$$

The slurry's total extinction coefficient, hereby, is obtained as the sum of both the water and the particles' extinction coefficient:

$$K_{total,e\lambda} = K_{bf,e\lambda} + K_{e\lambda} \quad (10)$$

The core-shell capsules' absorption and scattering coefficients, however, are based on the metallic shell structure's dielectric function. The metallic structures' dielectric function may be dissimilar from the bulk material due to size dependence [38]. Thus, modified Drude model can be employed to evaluate the dielectric functions since it varies the metallic shell's optical properties [36].

$$\varepsilon(w) = \varepsilon_{bulk}(w) + \frac{w_p^2}{w^2 + iw\gamma_\infty} - \frac{w_p^2}{w^2 + iw\gamma(R)} \quad (11)$$

where R, $\gamma(R)$ and γ_∞ can be calculated as [35,39]:

$$\gamma_\infty = \frac{1}{\tau_{bulk}} = \frac{1}{l_\infty/V_f} \quad (12)$$

$$R = \frac{1}{2}\left[(r_{shell}-r_{core})\left(r_{shell}^2 - r_{core}^2\right)\right]^{1/3} \quad (13)$$

$$\gamma(R) = \frac{1}{l_\infty/V_f} + \frac{AV_f}{R} \quad (14)$$

The materials' plasma frequency, Fermi velocity and mean free path are shown in Table 1. The optical parameters of the materials and water are also obtained from the literature [40–43].

The nanoencapsulated PCM slurry is presumed to be Newtonian, laminar, and incompressible. The governing equations are also described as:

$$\frac{\partial u}{\partial x} + \frac{\partial v}{\partial y} = 0 \quad (15)$$

$$u\frac{\partial u}{\partial x} + v\frac{\partial u}{\partial y} = -\frac{1}{\rho_{slurry}}\frac{\partial p}{\partial x} + \frac{\mu_{slurry}}{\rho_{slurry}}\left(\frac{\partial^2 u}{\partial x^2} + \frac{\partial^2 u}{\partial y^2}\right) \quad (16)$$

$$u\frac{\partial v}{\partial x} + v\frac{\partial v}{\partial y} = -\frac{1}{\rho_{slurry}}\frac{\partial p}{\partial y} + \frac{\mu_{slurry}}{\rho_{slurry}}\left(\frac{\partial^2 v}{\partial x^2} + \frac{\partial^2 v}{\partial y^2}\right) \quad (17)$$

$$\rho_{slurry}C_{p_{slurry}}\left(u\frac{\partial T}{\partial x} + v\frac{\partial T}{\partial y}\right) = k_{slurry}\left(\frac{\partial^2 T}{\partial x^2} + \frac{\partial^2 T}{\partial y^2}\right) - \frac{\partial q_r}{\partial y} \quad (18)$$

Subsequently, the boundary conditions are:
At the base:

$$\frac{\partial T}{\partial y} = 0 \quad (19)$$

At the outlet:

$$p = 0 \quad (20)$$

At the surface of panels:

$$u = v = 0 \quad (21)$$

At the top panel:

$$q = h(T - T_{amb}) + \epsilon\sigma\left(T^4 - T_{amb}^4\right) \quad (22)$$

At the inlet:

$$u = U_{in}, T = T_{in}, v = 0 \quad (23)$$

where h is defined as [45]:

$$h = 5.7 + 3.8w \quad (24)$$

Table 2
Thermophysical properties [47–51].

	H (J/kg)	ρ (kg/m^3)	C_p (J/kgK)	k (W/mK)
Liquid n-Octadecane		775	2660	0.149
Solid n-Octadecane	245,000	814	2140	0.35
Cu		8954	383	400
Ag		10,500	235	429
Al		2700	900	247
Au		19,320	128.8	314.4

Since the governing equations are based on the fluid's thermophysical characteristics, the phase change slurry's properties need to be determined. The detailed information can be found in the previous study of authors [31] on how to define the nano-encapsulated PCM slurry's thermophysical properties. Moreover, the mathematical modelling of pure nanofluids is investigated in the earlier studies of authors [30,46]. The thermophysical properties of the shell and PCM materials are also exhibited in Table 2.

The slurry, which has its initial temperature T_{in}, exits the collector by increasing its temperature as a result of the radiation in the collector. Hence, the slurry's temperature increment is defined as $T_{out} - T_{in}$. The

Fig. 2. 2D non-uniform mesh structure.

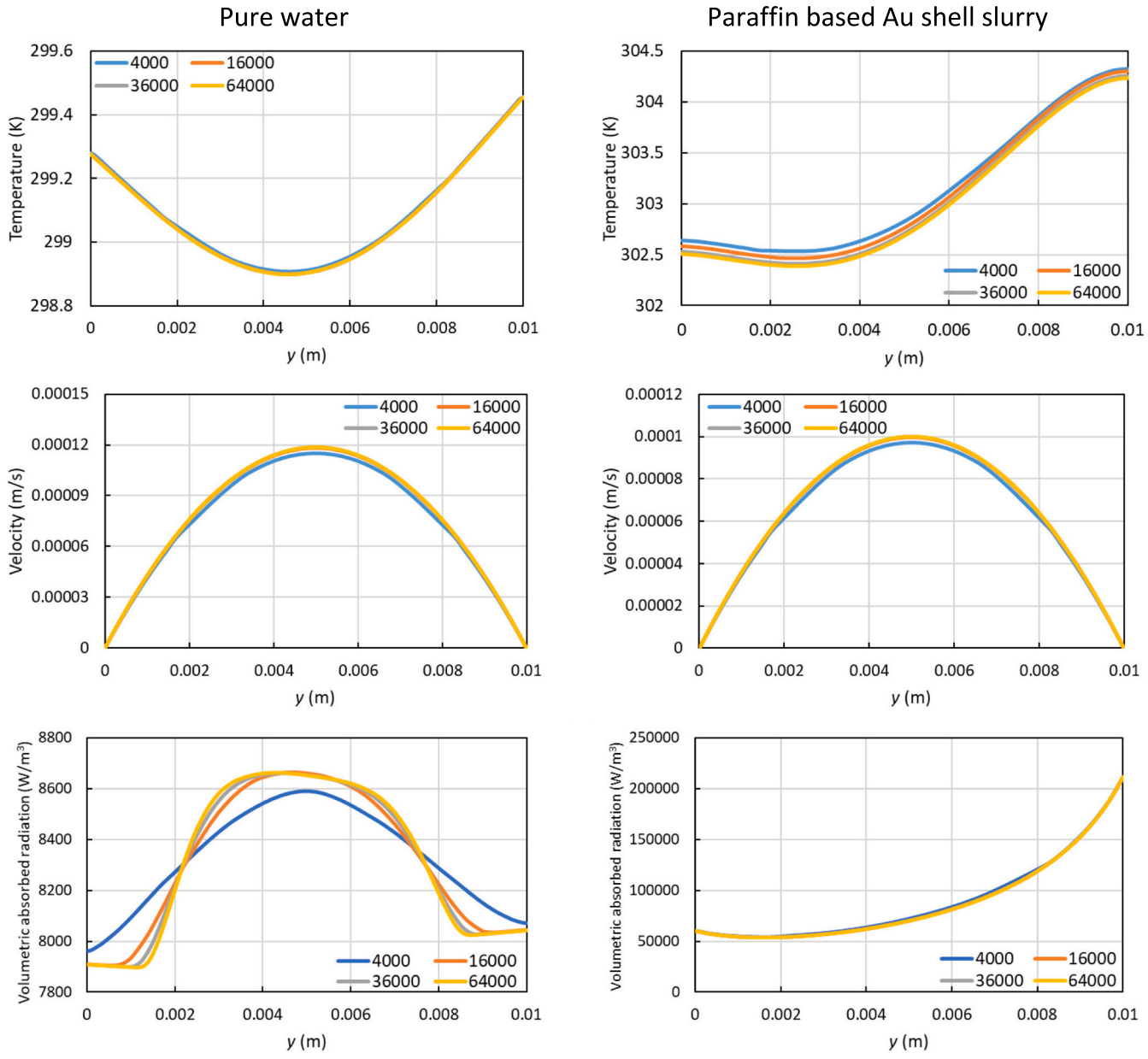

Fig. 3. Alteration of velocity, temperature, and volumetric absorbed radiation profiles for pure water and paraffin based Au shell slurry with different grid numbers.

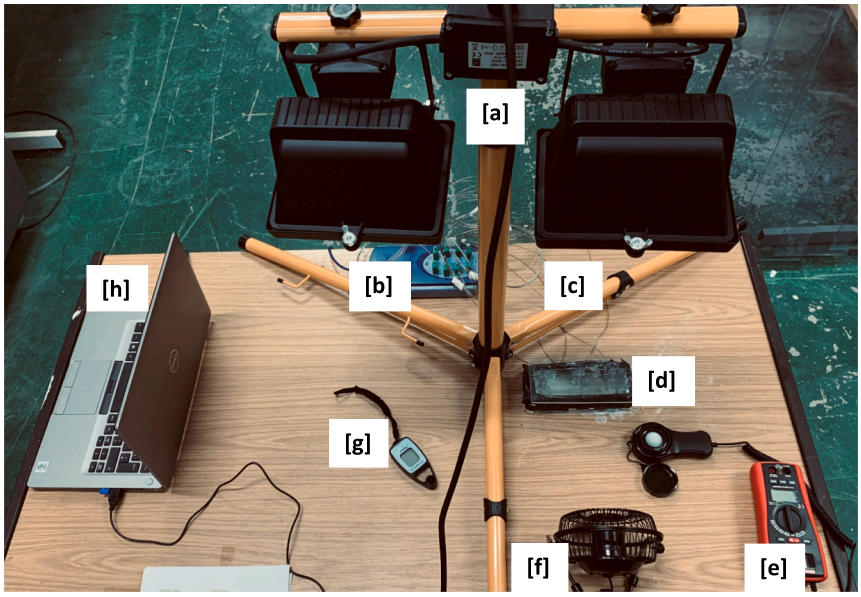

Fig. 4. Picture of the experimental setup (a) solar simulator, (b) data logger, (c) thermocouples, (d) heat storage cavity, (e) solar power meter, (f) fan, (g) anemometer, and (h) laptop.

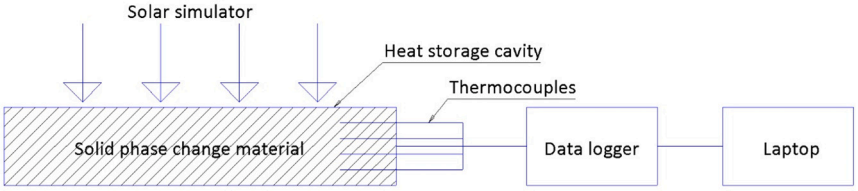

Fig. 5. Schematic layout of the experimental system.

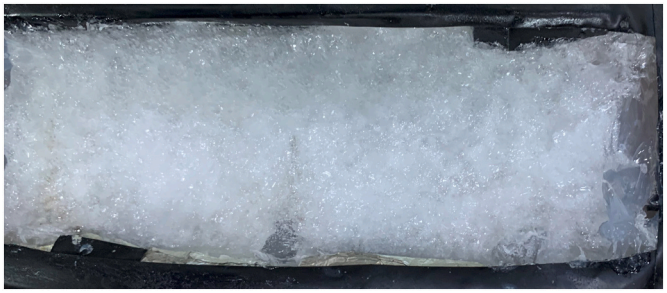

Fig. 6. Pure solid PCM (RT 28 HC).

amount of energy gain by the slurry due to the PCM's phase change effect is also equal to the enthalpy change of the slurry and is determined as [52,53]:

$$E = \dot{m}\,\Delta H \tag{25}$$

where ΔH depends on the ANSYS Fluent/computational findings.

2.1. Numerical procedure and grid independence test

The numerical model of governing equations was elaborated in the former works of authors [30,31,46]. This is a pressure based FVM (ANSYS Fluent 2020 R1). The Discrete Ordinates method was integrated for resolving the radiative transport equation which included the scattering, emitting, and absorbing points. The residual levels of the Discrete Ordinates and energy equations are also kept under 10^{-6} whereas for the other governing equations are under 10^{-5} in order to get better and more uniform results.

A grid sensitivity test is employed to get the solutions which are independent to the grid numbers. A non-uniform mesh structure is created (Fig. 2). The impacts of different grid sizes on the deviation of temperature, velocity, and volumetric absorbed radiation are illustrated in Fig. 3 by choosing various grid sizes that are 4000, 16,000, 36,000 and 64,000 using pure water and paraffin based Au shell slurry. The grid cells of 36,000, hence, is selected for the further calculations to reduce the computational time and get more precise outcomes.

3. Experimental procedure

The solid PCM's melting behaviour is experimentally analysed to validate the effective heat capacity model. It depends on the PCM's temperature and is given as [54]:

$$C_p = \begin{cases} C_{p,s} & T < T_s \\ \dfrac{C_{p,s} + C_{p,l}}{2} + \dfrac{H}{T_l - T_s} & T_s < T < T_l \\ C_{p,l} & T > T_l \end{cases} \tag{26}$$

The closed heat storage cavity, whose schematic diagram is presented in Fig. 4, is designed and the experimental system is set up as illustrated in Fig. 4 and Fig. 5. While the side walls and base are fully insulated, the upper plate is covered with the glass in order to collect the heat. The experimental set up also consists of solar simulator, data logger, thermocouples, heat storage cavity, solar power meter, fan, anemometer, and laptop. The heat storage cavity is filled with pure solid paraffin (RT 28 HC) which is suitable for solar applications due to the

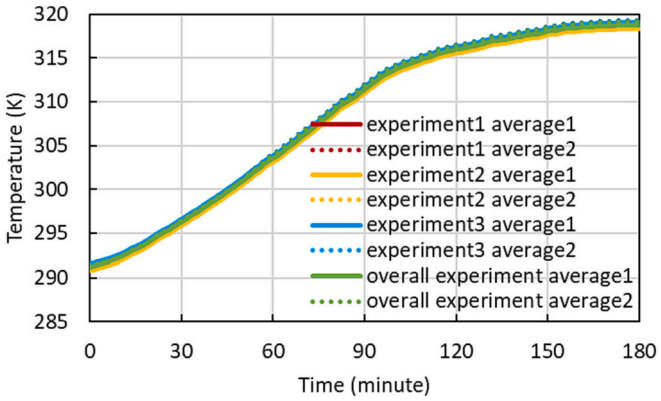

Fig. 7. Stability analysis of the experimental system.

phase change temperature and latent heat capacity (Fig. 6), and it is supplied by Rubitherm Technologies GmbH. A solar simulator using a 500 W halogen lamp which is similar to the one used in other studies such as [55] or [56] is applied to heat the solid PCM. The solar flux value reaching the glass surface is measured by the solar power meter as W/m^2, and the required heat flux is obtained by moving the solar simulator vertically. The thermocouples are also set in the cavity to measure the temperature change in the storage cavity and transmitted to the computer via a data logger to capture the data. Additionally, wind speed is measured with an anemometer, to compute the convective heat transfer coefficient on the top plate. Finally, the RT 28 HC's thermophysical properties can be found here [57].

4. Results and discussion

This part is separated into three sub-sections, beginning with the experimental findings and model validation followed by the examination of the numerical results.

4.1. Experimental results

The investigation of the solid PCM's melting behaviour is repeated three times under the same states for the constancy of the experimental results, and the PCM's average temperature is observed. Two various mean temperature values are employed: the first average temperature is achieved by using three different thermocouples, whereas six different thermocouples are utilized for the second average temperature. The same results are obtained from the three different experiments as exhibited in Fig. 7, and it also turned out to be the same when the two

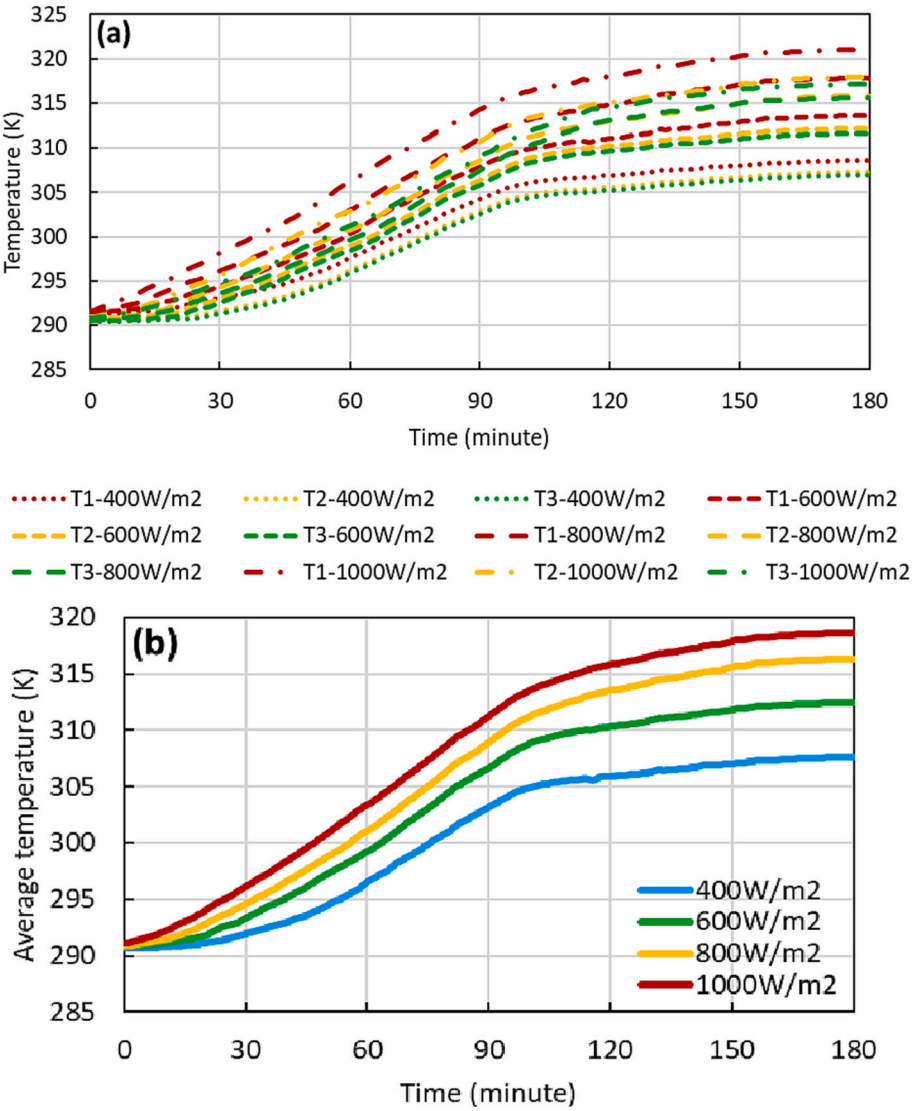

Fig. 8. Experimental analysis of (a) temperature distribution and (b) average temperature of the PCM within the cavity under various irradiances/heat fluxes.

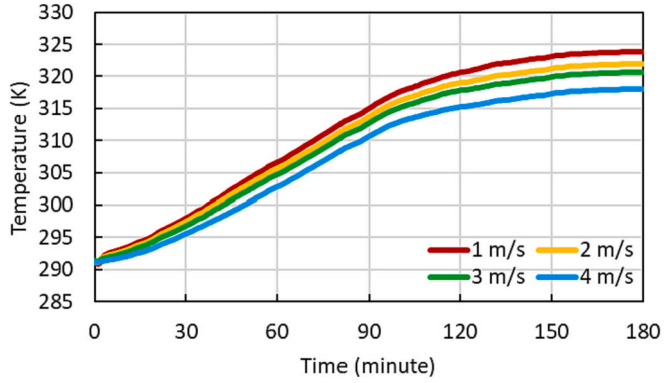

Fig. 9. Experimental analysis of PCM's average temperature within the cavity under various wind speed.

different average temperatures are compared. This indicates that the current experimental setup is reliable, and it is also uncovered that the working fluid reaches the steady state condition from the 150th minute. Furthermore, all the other walls of the cavity except the upper plate are covered with insulation matter to prevent the thermal losses. Moreover, since the experiment is carried out in a laboratory, that is, in an indoor status, there is no environmental effects such as no change in wind speed or clouding of the air. Additionally, the starting and finishing times of the experiment are the same for all cases. The cause for this is that the heated heat transfer fluid cools down during the same period. When these conditions are evaluated, it is seen that the situation as in Fig. 7 is obtained, and the standard deviation is under 1. Lastly, the time-dependent behaviour of the current repeatability test coincides with the behaviour of the stability verifying of the experimental study Hosseini et al. applied [58].

Fig. 8 indicates the various heat fluxes' influence on the PCM's temperature increment. The desired heat flow is obtained by moving the solar simulator in the vertical direction. Fig. 8(a) unveils the temperature variation of thermocouples positioned at different levels within the

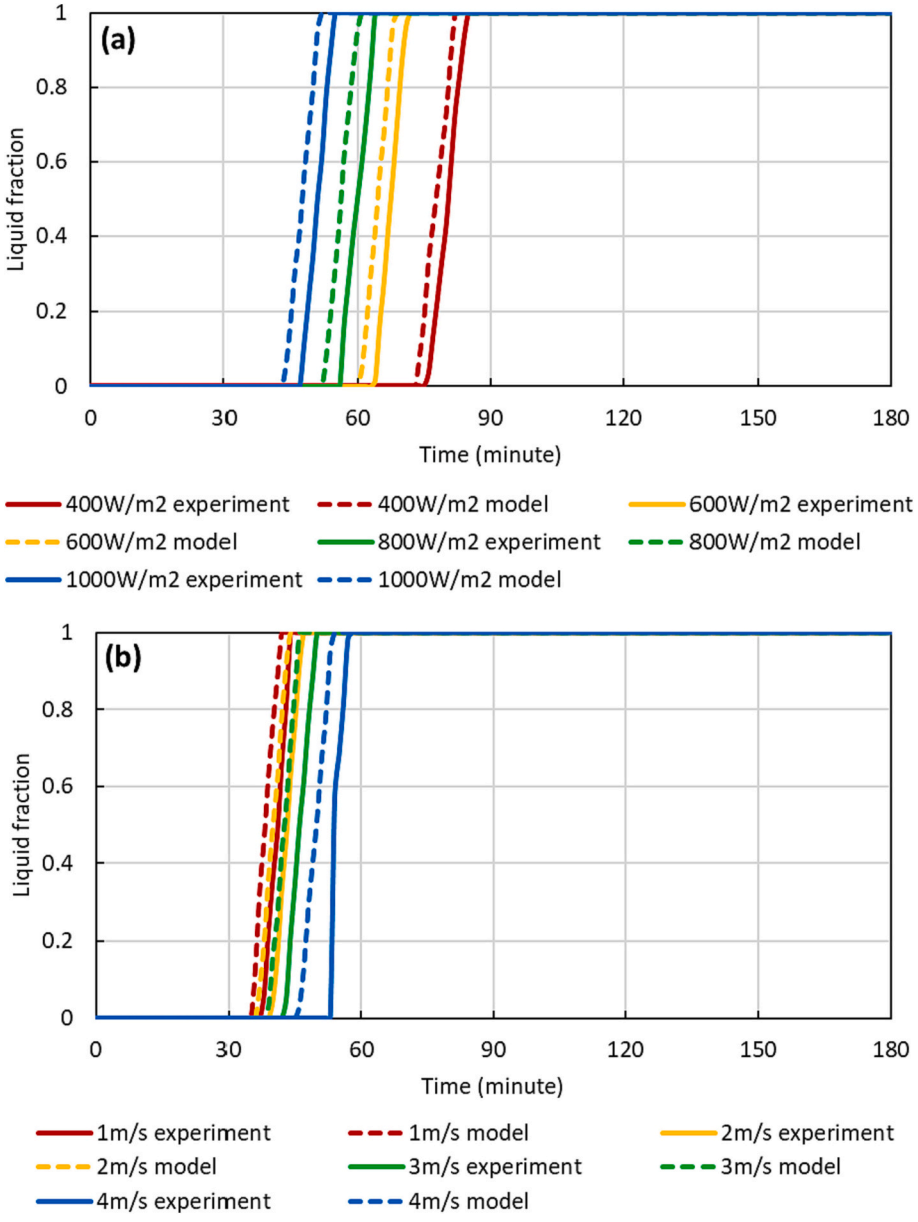

Fig. 10. Liquid fraction of the PCM within the cavity at (a) different irradiances and (b) different wind velocities.

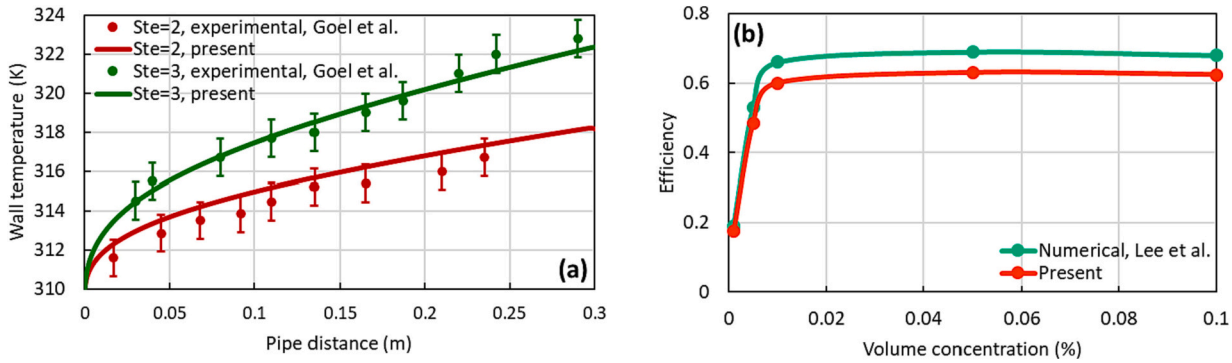

Fig. 11. Comparisons between current numerical model and literature results: (a) wall temperature along the flow direction [67], and (b) efficiency of the core/shell nanofluid as a function of volume concentration [68].

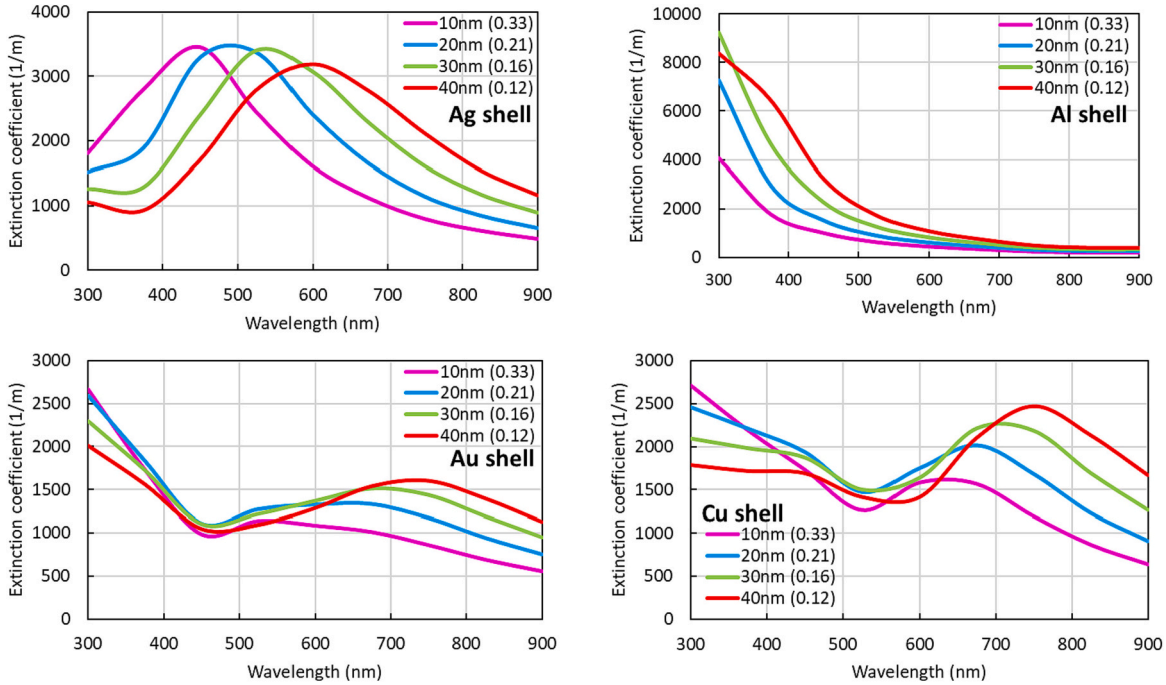

Fig. 12. Impact of core size (*SA:V*, m^{-1}) on extinction coefficient as a function of wavelength.

storage cavity. Accordingly, it is observed that as the depth of the cavity increases, the temperature increment diminishes from the top (T_1) to the bottom (T_3). The cause is that the PCM's temperature rise that starts to melt is higher than the solid or solid+liquid phase. The second reason is that as the cavity hight increases, the light intensity inside the cavity between the solar rays and PCM diminishes. It is also monitored that the temperatures measured from the middle and lower positions of the cavity are almost the same. This provokes a diminish in the phase change alteration due to the lessening in the temperature in the cavity as it is transmitted from the top to the bottom, resulting in insufficient temperature increment. In addition, augmenting the heat flux from 400 to 1000 W/m^2 accelerates the PCM's melting process, enhancing the heat gain of the liquid PCM more. The reason is that as the solar density enhances, the more radiation penetrates the solid PCM so that the amount of liquid PCM improves. The PCMs' average temperature, thus, improves with enhancing the heat flux (Fig. 8(b)). This mean temperature, which augments as a function of time, is in agreement with the research of Sodhi et al. [59] and Siyabi et al. [60] who analysed the PCM's charging.

Another factor affecting the temperature rise and phase transition is the wind speed. The increase or decrease of the wind velocity influences the energy storage material's thermal behaviour. As the fan is moved horizontally and brought closer to the storage cavity, the speed increases. Thus, as indicated in Fig. 9, improving the wind velocity from 1 to 4 m/s decreases the PCM's average temperature increment. Enhancing the wind speed increases the thermal losses from the storage cavity to the atmosphere. This is because the forced convection currents to the glass surface of the storage cavity are more accumulated. Heat losses to the environment, hence, increase, causing the solid PCM to melt later and negatively affecting the temperature gain. This decrease in the PCM's performance is encouraged by the investigation of Liu et al. [61] and Khanna et al. [62].

4.2. *Validation*

The liquid fraction of the experimental and current computational findings is compared to validate the specific heat capacity model. The melt fraction takes place during the phase change and shows the amount of melting. It can also be defined as follows [63]:

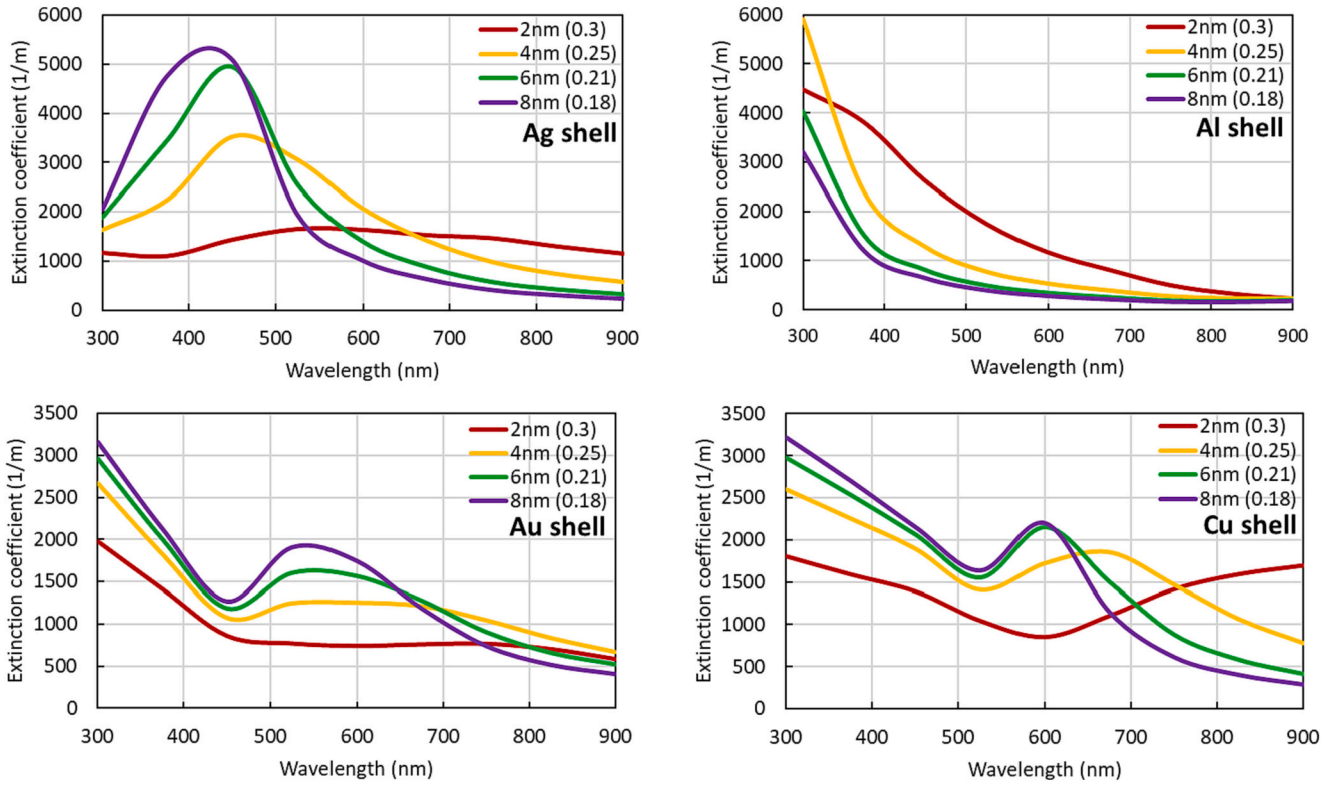

Fig. 13. Impact of shell thickness size (*SA:V*, m^{-1}) on extinction coefficient as a function of wavelength.

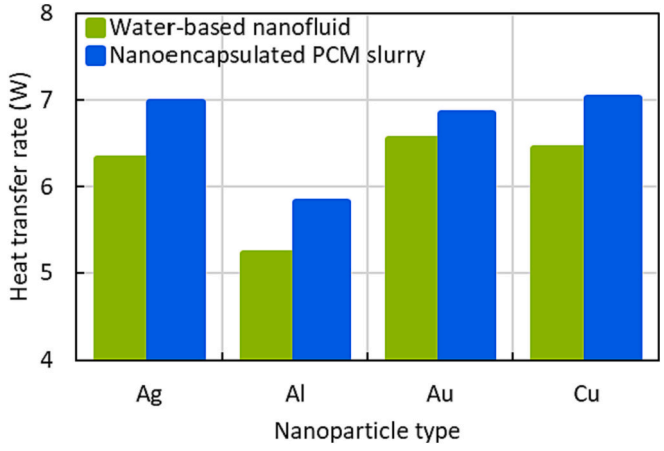

Fig. 14. Comparison of nanofluid and nanoencapsulated PCM slurry on thermal performance.

$$\gamma = \begin{cases} 0 & T < T_s \\ \dfrac{T - T_s}{T_l - T_s} & T_s < T < T_l \\ 1 & T > T_l \end{cases} \tag{27}$$

Fig. 10 (a) and (b) display the influences of heat flux and velocity on the liquid fraction, respectively. It is displayed that there is a good consistency between the numerical model and the experimental results. Furthermore, the current melt fraction's behaviour as a function of time is consistent with that of Sodhi and Muthukumar [64] and Tao et al. [65]. Moreover, the improved heat flux/wind speed and time-dependent changes of the liquid fraction also coincide with the findings of Liu et al. [61]. The results also clearly display that the mushy state (solid and liquid PCM) depends on the environmental conditions. As the heat input augments from 400 to 1000 W/m^2, the solid PCM starts to melt earlier (Fig. 10(a)). Thus, the liquid PCM's temperature rise further augmented (Fig. 8(b)). When the wind speed, on the other hand, increases from 1 to 4 m/s, the melting time becomes longer (Fig. 10(b). It means that the PCM begins to slow down further, causing a decrease in heat gain (Fig. 9).

Moreover, the statistical analysis is shown to carry out a comparison between the numerical and experimental results in order to assess the reliability of the simulations. The mean absolute error (*MAE*) is calculated as [66];

$$MAE = \frac{1}{N_{data}} \sum_{n=1}^{N_{data}} \left(T_{num,n} - T_{exp,n} \right) \tag{28}$$

where N_{data} is the number of temperature values recorded in the experiment, T_{num} and T_{exp} are numerical and experimental results, respectively. Therefore, it is noticed that the numerical results closely match with the experimental data set with the mean absolute error of 1.5 in the phase change range/process as shown in Fig. 10.

An experimental study conducted by Goel et al. [67] is also used to further validate the specific heat capacity model of microencapsulated PCM slurry. A horizontal pipe of diameter 3.14 mm and length 0.3 m is adopted for the experiment. N-eicosane and water are selected for the PCM and water, respectively. The different Stefan number is used to define the ratio of the sensible heat capacity of the suspension to its latent heat capacity. As illustrated in Fig. 11(a), the current simulation results match well with the benchmark model. The accuracy of the radiation modelling is selected by Lee et al. [68], who used the SiO_2/Au core/shell confinement dispersed in water in their work. The solar collector's top wall is exposed to solar radiation of 1367 W/m^2 and has the heat losses to the ambient as 10 W/m^2K. The fluid's inlet temperature equals to the ambient temperature as 293.15 K. There is a good agreement between the present and the benchmark findings, with an average discrepancy of less than 8.5 % (Fig. 11(b)).

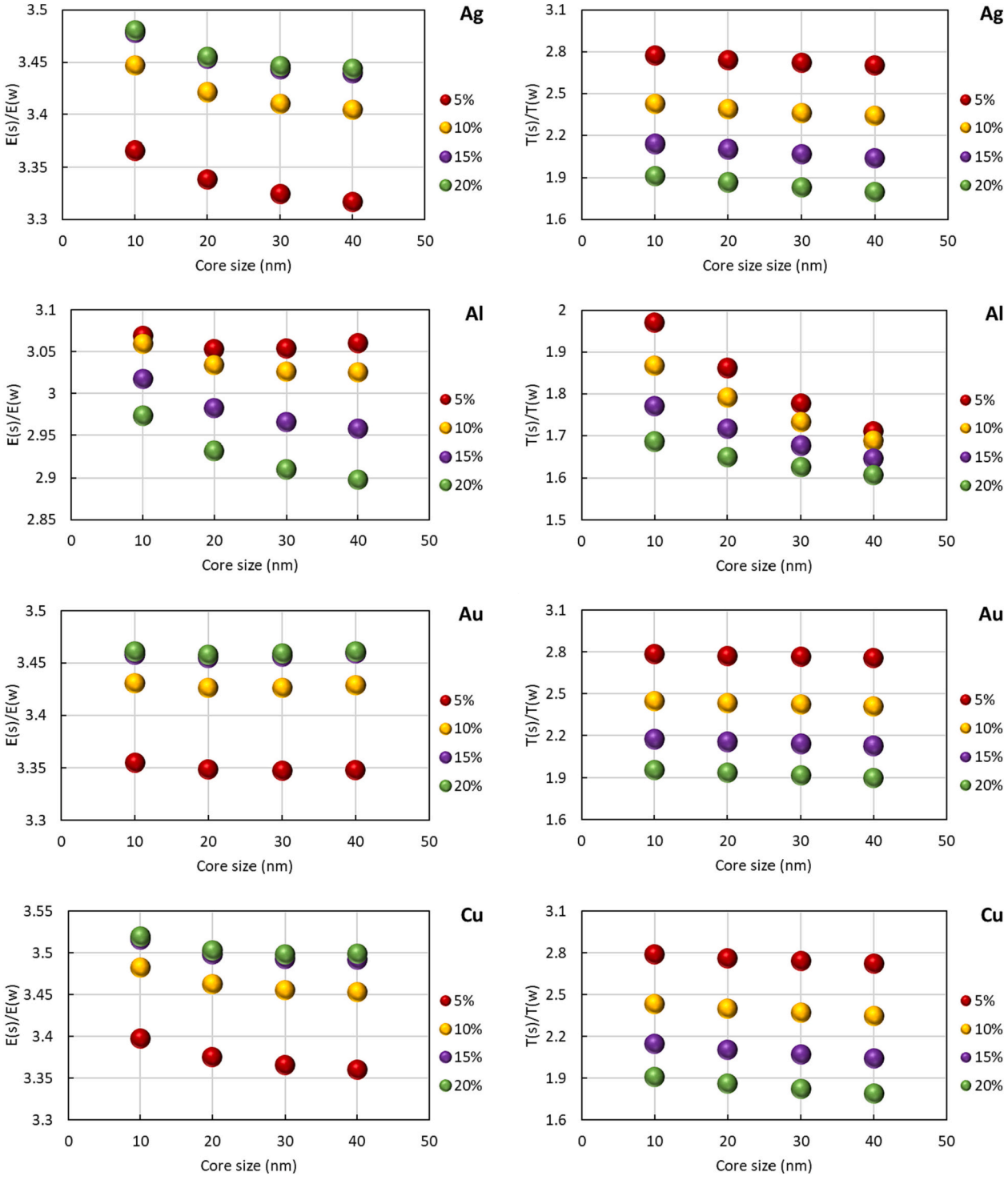

Fig. 15. Impacts of PCM mass concentration and shell material on energy gain (left column) and temperature increment (right column) ratios (s and w represent the nanoencapsulated PCM slurry and pure water, respectively).

4.3. Numerical results of photothermal conversion performance

Since there is a good agreement of validation cases for radiation and effective heat capacity models, this study can be expanded in order to comprehensively examine the photothermal conversion performance. This section first highlights the core/shell structures' optical properties, followed by the impacts of the shell thickness, core size, type of shell materials and shell concentration on the system's thermal capability. The size of the nano capsules is compatible with other studies such as [69–72].

4.3.1. Effect of core size on optical properties

Encapsulated PCMs are created by using copper (Cu), silver (Ag), gold (Au), and aluminium (Al) materials as shell structures. Since the shell and core materials have unlike optical characteristics, the encapsulated PCMs' optical behaviour also differs.

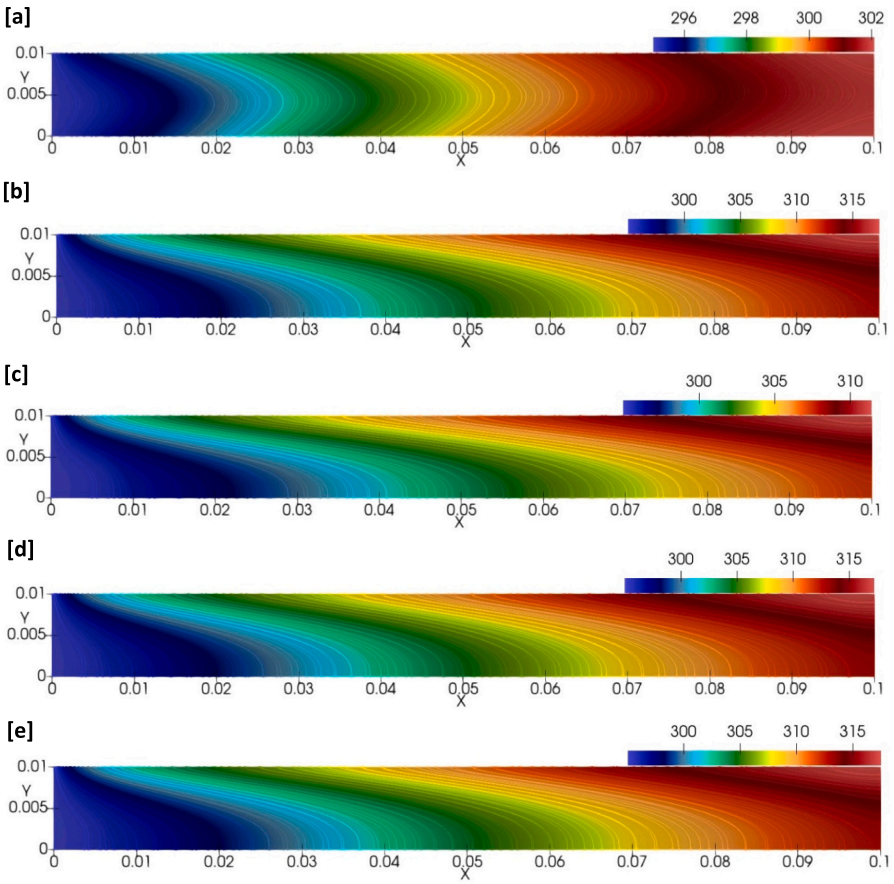

Fig. 16. Temperature (K) profiles at PCM mass concentration of 5 % core diameter of 10 nm: (a) pure water, (b) paraffin/Ag slurry, (c) paraffin/Al slurry, (d) paraffin/Au slurry, and (e) paraffin/Cu slurry.

Fig. 12 unveils the influence of the core size as a function of wavelength on extinction coefficient with different shell materials. The influence of dissimilar shell materials and enhanced core size on the absorption and scattering cross sections at wavelengths occurs due to the surface plasmon resonance impact. Metallic shell materials have free electrons on their surface. Under the influence of sunbeam in this layer, the peak positions are formed by the vibration frequency between electrons and radiation. As indicated in Fig. 12, it is observed that the peak positions gradually shift to red depending on the enhancing core size (decreasing *SA:V*). This shifting with augmenting the nano capsule is also revealed by Wu et al. [37] and Lv et al. [35]. When the core size of paraffin/Cu and paraffin/Au shell confinements is 40 nm, that is the *SA:V* is minimum as 0.12 m^{-1}, the resonance peaks in the infrared waveband increase, while the resonance peaks of the Paraffin/Ag capsule take the maximum value in the visible band. Due to the stronger optical properties of Ag and Cu metallic nanoparticles, peak formations are more pronounced than other shell materials. It is also observed that the improvement of the core size enhances the mean attenuation coefficient.

4.3.2. *Effect of shell thickness size on optical properties*

Fig. 13 indicates the influence of shell thickness as a function of wavelength on attenuation coefficient with various paraffin-based shell materials. The metallic nanoparticles' free electrons activate the surface plasmon under the influence of solar radiation. Thus, the extinction peaks formation is observed. It is illustrated in Fig. 13 that the enhancement in the shell thickness enlarges the nano capsules' total size, reducing the *SA:V* and the peak positions are shifted to blue. It is encouraging to compare this finding with that found by Duan et al. [38] and Duan et al. [73] who discovered that wave band is blue shifted with enhancing shell thickness. It is found that as the shell material's thickness enhances from 2 to 8 nm, that is the *SA:V* diminishes from 0.3 to 0.18 m^{-1}, the paraffin/Ag nano capsules' peaks shift from 525 to 450 nm wavelength. Even though the trends in the attenuation coefficients of Cu and Au-shelled paraffin nano capsules seem to be the similar, it is observed that the paraffin/Cu structure's peak positions are more pronounced due to the stronger optical characteristics of Cu nanoparticles. In the paraffin/Al nano capsule, both the increase in wavelength and the augmentation in the shell thickness cause a diminish in the attenuation coefficient. It is clearly noted in the Ag shell structure that while the extinction coefficient augments up to the wavelength at which the resonance peak is maximum, it is seen to diminish from this wavelength. As seen in Fig. 13, although the surface plasmon resonance effect improves light absorption, this enhancement is wavelength dependent.

4.3.3. *Comparison of thermal performance of nanofluid and nanoencapsulated PCM slurry*

Thermal performance of nanofluid and nanoencapsulated PCM slurry as working fluids is compared. Cu/water, Au/water, Al/water, and Ag/water nanofluids are achieve by dispersing Cu, Au, Al, and Ag nanoparticles in pure water, respectively. Paraffin selected as the PCM is encapsulated by using these nanoparticles as shell material and uniformly dispersed in pure water, thus the slurry is obtained. The heat transfer rate is employed to compare the thermal ability of these two different fluids in the collector [74]:

$$\dot{Q} = \dot{m}\Delta T\left[(1-c_m)C_{p,water} + c_m C_{p,PCM}\right] + \dot{m}c_m H \tag{29}$$

As described in Fig. 14, the heat transfer rates of water based Ag, Au, Cu and Al nanofluids 6.89, 5.86, 7.05 and 6.99 W, respectively. With the

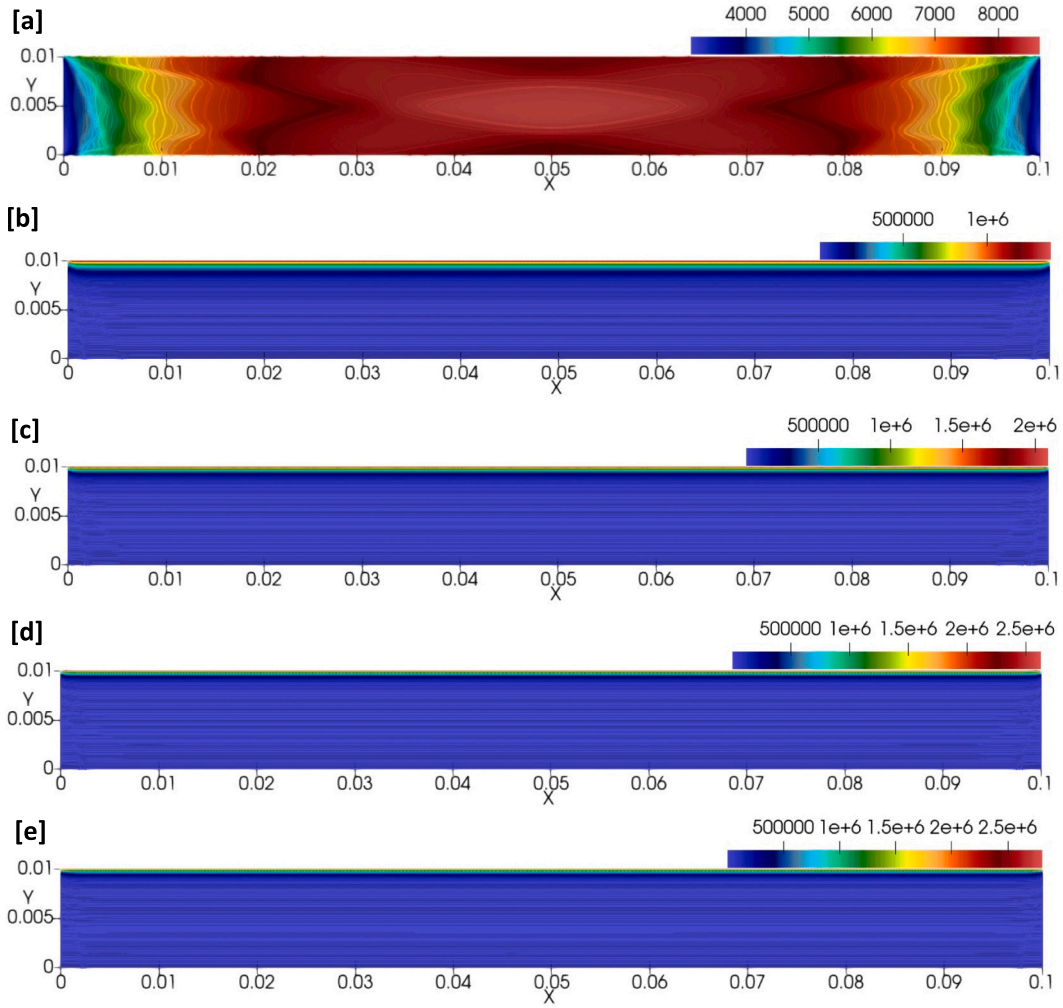

Fig. 17. Volumetric absorbed radiation (Wm^{-3}) profiles at PCM mass concentration of 5 % for paraffin/*Al* slurry with changing core size: (a) pure water, (b) 10 nm, (c) 20 nm, (d) 30 nm, and (d) 40 nm.

addition of Paraffin@Ag, Au, Cu and Al nanocapsules to pure water, the enhancement in heat transfer augments as 6.18, 13.38, 10.8 and 11.33 %, respectively. The paraffin's mass concentration is the lowest amount, 5 %, for this enhancement. This augmentation is taken place due to the PCM's high latent heat capacity. These results reflect those of Languri and Rokni [74] who reported that better heat transfer could be realised with the addition of PCM to water. Moreover, since *Al* has the lowest thermal conductivity, its enhancement has the lowest when compared to other shell materials.

4.3.4. Combined effects of core dimension and shell material type on thermal performance

The influence of combined shell type and core size on optical properties is analysed in Section 4.3.1. In this part, the impact on the thermal capability of the collector is examined by considering the thermophysical properties along with the optical characteristics. The properties that affect the nanoencapsulated PCM slurry's thermal performance can be defined as the shell material, core size, and PCM mass concentration. The PCM's mass concentrations are examined as 5, 10, 15 and 20 %.

The nanoencapsulated PCMs' attenuation coefficient varies depending on the shell type material in the wavelength range as indicated in Fig. 12. Especially when the paraffin/*Al* nano capsule's core size is 30 and 40 nm, it has a higher attenuation coefficient than other shell materials. Since *Al* nanoparticle has the lowest thermal conductivity coefficient, however, as a result of insufficient heat transfer of paraffin/*Al* nano capsules dispersed in pure water, the temperature rise is at the lowest level and the temperature increment ratio is the minimum as seen in Fig. 15. Thus, the paraffin/*Al* slurry's heat gain is also low.

In addition, the paraffin/Ag nano capsule's average extension coefficient is higher than the paraffin/Au and paraffin/Cu nano capsules at the specified wavelength. This allows it to absorb more solar radiation. This, on the other hand, causes the collector's upper wall temperature to be slightly higher in paraffin/Ag slurry than other slurry types. Hence, by increasing the thermal losses from the collector to the surrounding, it prevents further enhancement the slurry's heat gain. Furthermore, it is found that the improvement in the temperature and heat gain diminish with the improvement of the core size (Fig. 15). Since increasing the dimension of the nucleus increases the nano capsule's total size, the particle's volume improves at constant concentration. The increase in volume reduces the *SA:V* of the capsule, allowing the nano capsules dispersed in water to clump together. This diminishes the heat transfer between the water and capsules, negatively affecting the performance. This study supports evidence from previous observation by Ashraf et al. [75] who revealed that augmenting the capsule size and agglomeration weakens the nanocomposites' performance. However, it is observed that the paraffin/*Al* slurry's heat gain enhances with the size enhancement in some cases. The probable reason for this is that although the enthalpy gain declines in all other cases, the mass flow rate is higher in these special cases than in the others. For example, the heat energy ratios decreases by 5.3, 15.9, 5.15, and 5 %, respectively, as the particle size of

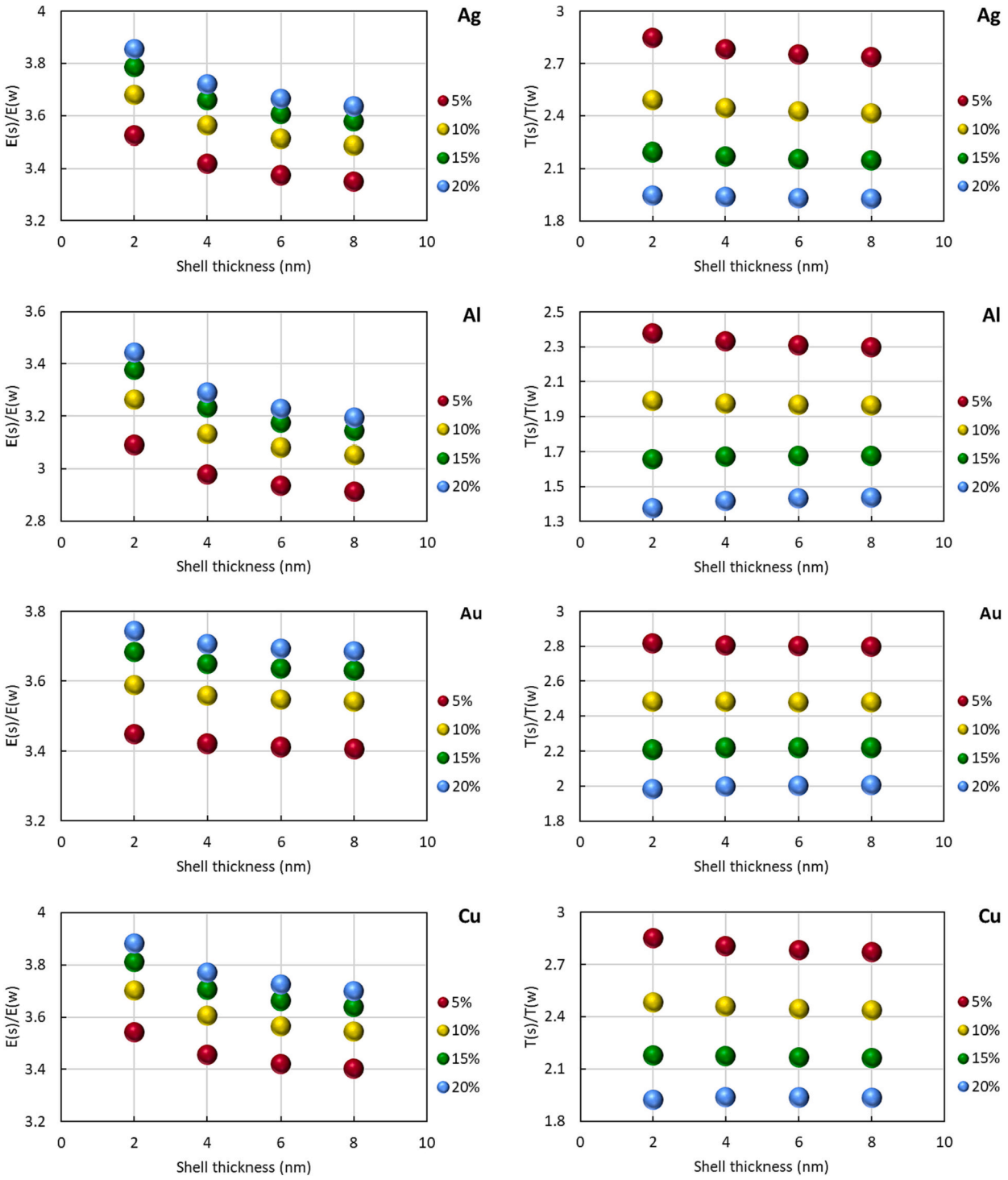

Fig. 18. Impacts of PCM mass concentration, shell thickness and shell material on energy gain (left column) and temperature increment (right column) ratios (*s* and *w* represent the nanoencapsulated PCM slurry and pure water, respectively).

Paraffin@Ag, Au, Cu and Al composite PCMs enhances from 18 to 48 nm at PCM mass concentration of 5 %.

Another important point is that improving the mass concentration from 5 to 20 % at fixed capsule size led to the heat gain's improvement as demonstrated in Fig. 15. This allows the PCM, which is a higher latent heat of fusion, to absorb more energy. This result supports the idea of Bohdal et al. [53] who found that the microencapsulated PCM slurry's enthalpy gain enhances as the PCM mass concentration increases at the working conditions. Surprisingly, the opposite is true for paraffin/*Al* slurry. This can be explained by the decrease in the mass flow rate depending on the slurry's thermophysical properties that is consisted with the investigation of Jia et al. [17]. Accordingly, as supported by the research of Languri and Rokni [74] and Jia et al. [17], it is found that the slurry's temperature increment diminishes with high heat storage capacity as a result of the enhancement in the PCM mass concentration at the rigid particle dimension.

The temperature profiles of various fluids in the collector are exhibited in Fig. 16. In the system used as the working fluid of pure

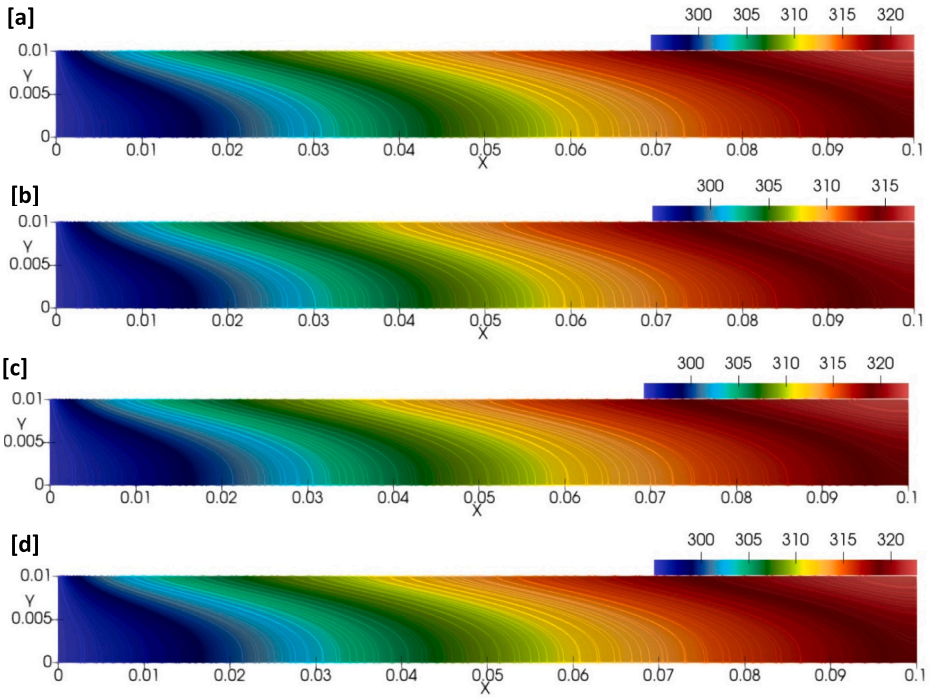

Fig. 19. Temperature (K) profiles at PCM mass concentration of 5 % and shell thickness: (a) paraffin/Ag slurry, (b) paraffin/Al slurry, (c) paraffin/Au slurry, and (d) paraffin/Cu slurry.

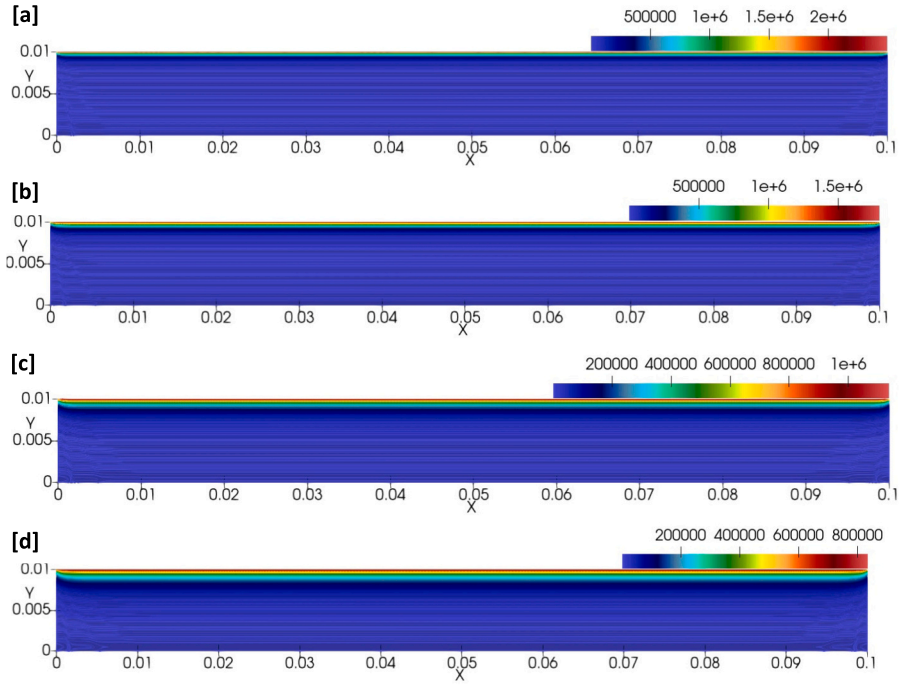

Fig. 20. Volumetric absorbed radiation (Wm^{-3}) profiles at PCM mass concentration of 5 % for paraffin/*Al* slurry with changing core size: (a) 2 nm, (c) 4 nm, (d) 6 nm, and (d) 8 nm.

water, it is monitored that the collector's temperature increment is the lowest due to the insufficient optical properties of the water (Fig. 16(a)). This causes a more uniform temperature circulation in the collector. It is also examined that the heat gain in slurries formed by adding nano capsules to distilled water is considerably higher than that of pure water (Fig. 16(b-e)). The lower optical and thermophysical properties of paraffin/*Al* slurry compared to other slurry types, however, causes a higher temperature increment (Fig. 16(c)). It is earlier that the paraffin/Ag (Fig. 16(b)) and paraffin/Cu (Fig. 16(e)) slurries begin to warm through the collector. This is the result of their high extinction coefficient and thermal conductivity.

Fig. 17 explains the impacts of varying core size of the paraffin/*Al* slurry on the volumetric absorbed radiation. Due to the pure water's low attenuation coefficient, heat generation from radiation is uniformly

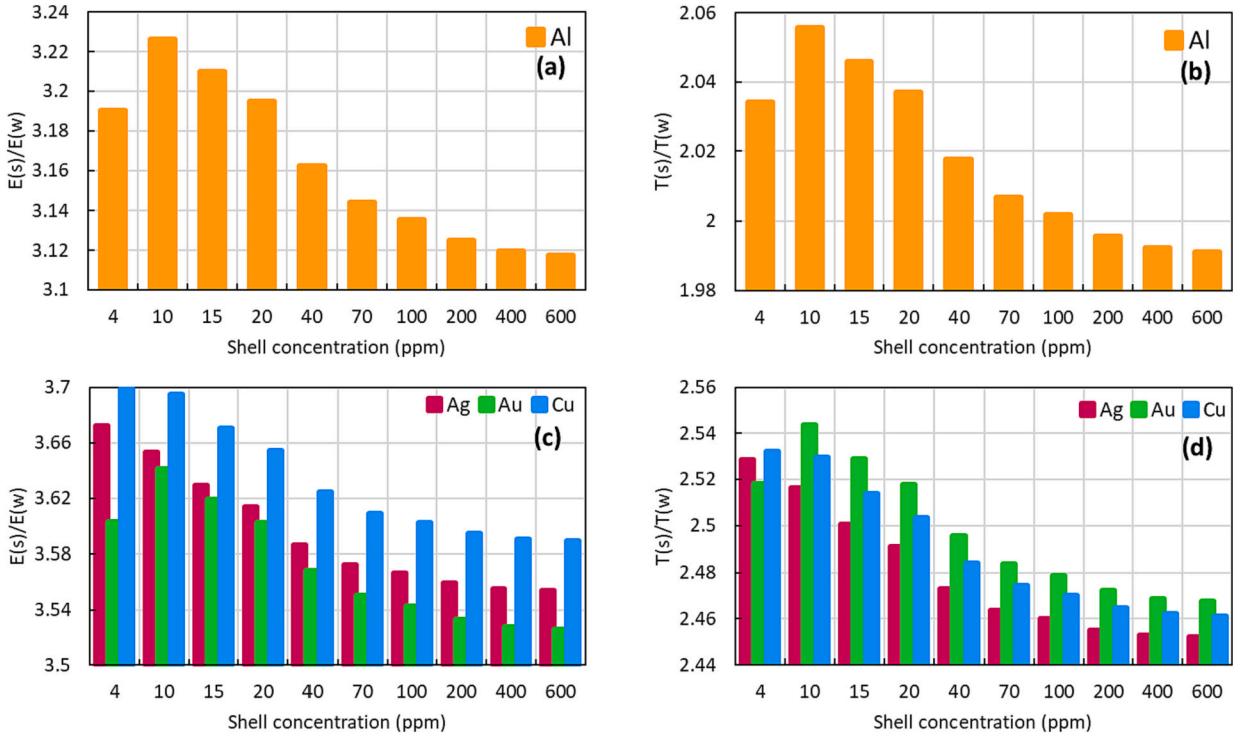

Fig. 21. Impacts of shell concentration and shell material type on energy gain (left column) and temperature increment (right column) ratios (*s* and *w* represent the nanoencapsulated PCM slurry and pure water, respectively).

obtained by penetrating more of the solar radiation into the collector (Fig. 17(a)). Due to the nano capsules' high optical properties, the heat transfer fluid's radiation absorption capacity, whose extinction coefficient is improved, increases much more than pure water (Fig. 17(b-e)). The greater absorption of radiation at the vicinity of the upper wall of the nano capsules causes the heat generation to diminish towards the collector's base. Thus, maximum heat generation and radiation heat flux are achieved around the upper wall. This finding was also reported by Kazaz et al. [46]. Besides, parallel to Fig. 12, the augmentation in the core size improves more heat capacity, resulting in an increment in the average heat generation in the collector (Fig. 17(b-e)).

4.3.5. Combined effects of shell thickness and shell material type on thermal performance

Section 4.3.2 shows the effect of combined shell type and shell thickness on optical properties in the wavelength range. Another factor impacting the performance features in thermal systems is the fluid's thermophysical properties. Therefore, the impact of combined thermophysical and optical behaviours of the fluid on the collector capacity should be examined. The host fluid, shell material, shell thickness and PCM mass concentration can be defined as structures that create this combined effect. PCM mass concentrations is also chosen as 5, 10, 15 and 20 %.

It is stated in Fig. 13 that the nanoencapsulated PCMs' extinction coefficient varies in the wavelength range depending on the type and thickness of the shell material. Since paraffin/*Al* capsules and *Al* particles have low average extinction coefficients and thermal conductivities, respectively, the paraffin/*Al* slurry has the lowest thermal performance as in Fig. 18. It is observed that the decrease in the thermal performance of the paraffin/Ag slurry is huge compared to the paraffin/Au and paraffin/Cu slurries due to the improvement in the shell thickness at the fixed PCM mass concentration. The reason for this, as seen in Fig. 13, shows that paraffin/Ag nano capsules with better mean attenuation coefficient can absorb radiation more. This situation, however, effects the heat losses from the collector to the environment to increase a little more, allowing the paraffin/Ag slurry to have this kind of performance.

Besides, as mentioned in Section 4.3.4, improving the capsule size negatively affects the collector's performance. Likewise, increasing the shell thickness increases the nano capsules' overall size. This state which causes an increase in the particle volume at a constant concentration, on the other hand, leads to the *SA:V* of the capsules to narrow, creating agglomeration in the base fluid, reducing the slurry's average thermal performance. This case coincides with work of Ashraf et al. [75] who observed that the positive effect of nanocomposites decreases as the particle size increases.

Improving the PCM mass concentration from a constant shell thickness of 5 to 20 % permits the PCM to absorb more heat during the phase change, resulting in improved heat recovery rates as seen in Fig. 18. This finding agrees with those obtained by Qiu et al. [18] who reported that the fluid's heat absorption augments with enhancing the mass concentration. However, it is found that this augmentation in concentration causes a decrease in the temperature increment rate. This is likely since the temperature change remains almost constant as the PCM changes phase due to enhancing storage capacity. This is encouraged by the study of Jia et al. [17] who obtained that slurry's exit temperature from the collector declines as the PCM mass concentration enhances from 0.05 to 0.2 at the same working conditions.

Fig. 19 shows the various working fluids' influences on temperature. As indicated in Fig. 16, pure water is the heat fluid with the lowest temperature increment. By adding different types of shell materials with a shell thickness of 8 nm to pure water, the fluid's capability to absorb solar energy has improved. The fact that the shell materials have a metallic structure allows radiation and free electrons to interact, thus enhancing the temperature of the slurry by colliding the capsules with each other. As displayed in Fig. 19(a, c, d), when the thickness of paraffin/Ag, paraffin/Au and paraffin/Cu slurries thickness is 8 nm, it is noticed that the greatest temperature is the same since the mean attenuation coefficients are close to each other. It is found that the temperature increment of the paraffin/*Al* slurry is lower than the other slurries due to the paraffin/*Al* capsule's poor attenuation coefficient and

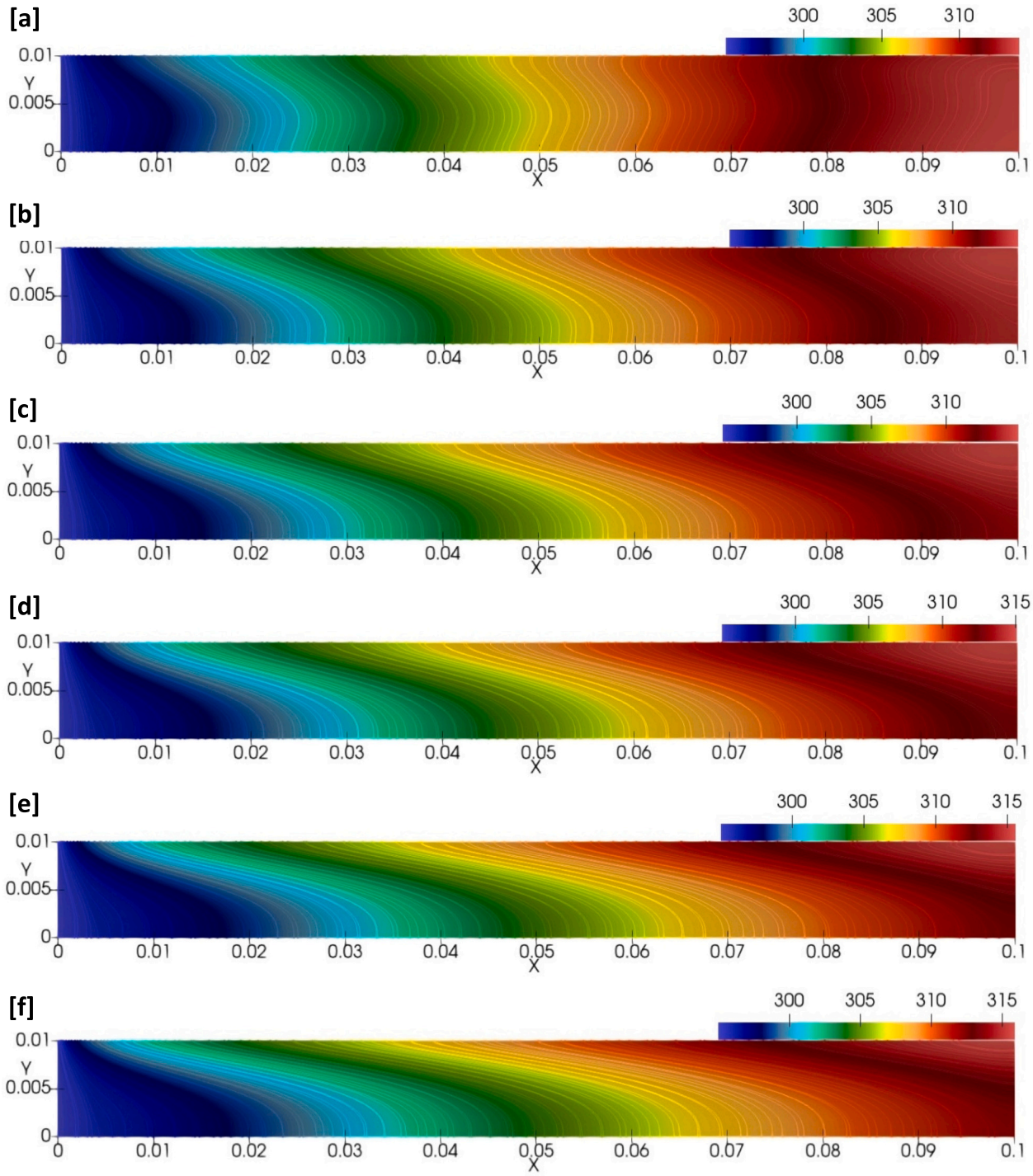

Fig. 22. Temperature (K) profiles of paraffin/*Al* slurry at different shell concentrations: (a) 4, (b) 10, (c) 15, (d) 20, (d) 40, and (e) 70 ppm.

low thermal conductivity (Fig. 19(b)).

The impact of different shell thickness on volumetric absorbed radiation is indicated in Fig. 20. As explained in Fig. 13, the increase in shell thickness of paraffin/Al nano capsules causes a diminish in the average attenuation coefficients. This is evident in Fig. 20, where the paraffin/*Al* slurry causes a decrease in the absorption capacity of radiation. Thus, it leads to the heat gain of the slurry to deteriorate due to the decrease in temperature increment.

4.3.6. Effect of shell volume concentration on thermal performance

The shell concentration is another feature that affects system performance. In this section, the combined effect of different volume concentrations with different types of shell materials is analysed.

Enhancing the shell volume concentration permits the nano capsules to absorb more solar light, improving the slurry's temperature increment (Fig. 21(a, c)). Thus, the energy recovery of the fluid is also improved (Fig. 21(b, d)). However, it is clearly displayed in Fig. 21 that augmenting the volume concentration from 4 to 10 ppm improves the system performance, while an increase in the volume concentration after 10 ppm adversely alters the collector's thermal capacity. Nano capsules consisting of shell structures with metallic properties can collide with each other by displacing them in the base fluid in a similar

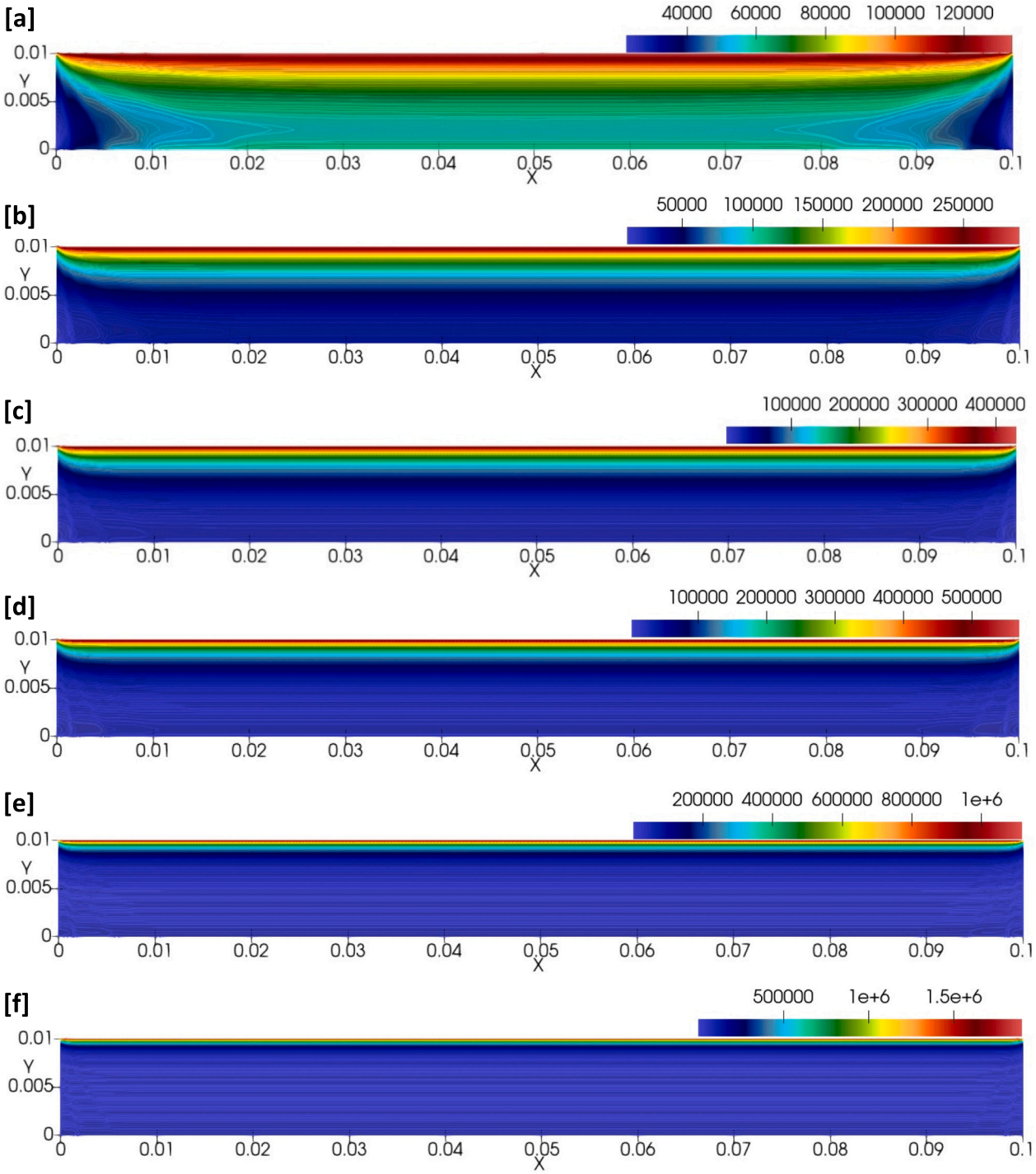

Fig. 23. Volumetric absorbed radiation (Wm^{-3}) profiles of paraffin/*Al* slurry at different shell concentrations: (a) 4, (b) 10, (c) 15, (d) 20, (d) 40, and (e) 70 ppm.

way to nanoparticles. This augmentation in volume concentration leads to enhancement in the amount of metallic nanoparticle molecules in the shell. Although this improves the interface impacts and intermolecular collisions of nano capsules, it causes agglomeration of nano capsules and negatively affects the fluid's temperature increment in the collector. Accordingly, it also accelerates the thermal losses from the collector to the atmosphere by increasing the heat gains of the nano capsules at the vicinity of the panels of the collector. Depending on these, a diminish is observed in the system's overall performance. This negative outcome displays the idea of Kazaz et al. [46] who described that reduced collision of particles leads to convection streams' weakening. As illustrated in Fig. 21, when the shell particle concentration enhances from 4 to 600 ppm, the storage enhancement of paraffin@Cu, Au, Al, and Ag core/shell PCM based heat transfer fluid diminishes by 7.27, 7.41, 6.82, and 11.11 %, respectively.

It is also stated in Fig. 21 that the paraffin/*Al* slurry's thermal capacity (Fig. 21(a, b)) is lower than the other slurry types (Fig. 21(c, d)). As explained in the previous sections, it allows paraffin/Ag, paraffin/Au, and paraffin/Cu slurries to have better capacity due to low thermal conductivity and optical properties of Al particles.

Different volume concentrations' impacts on temperature and volumetric absorbed radiation profiles are displayed in Fig. 22 and Fig. *23*,

respectively. Enhancing the volume concentration increases the slurry's capacity to absorb solar energy. Due to the increased radiation intensity within the collector, the heat production in the slurry (Fig. 23) augments, improving the temperature increment ratio (Fig. 22). However, an augmentation in the volume concentration from 4 to 70 ppm reduces the penetration of the radiation in the collector and causes it to concentrate around the upper wall, allowing more heat generation to occur around the collector's top panel (Fig. 23(a-f)). This causes the collector's average upper wall temperature to boost, thus accelerating the heat losses. This alters the slurry's mean exit temperature from the collector to decrease (Fig. 22(a-f)). The similar finding was also reported by Bhalla and Tyagi [76] who reported that as the volume concentration augments, the fluid's temperature around the top wall to increase.

5. Conclusions

The photothermal conversion performance of a direct absorption solar energy storage system using nanoencapsulated PCM slurry was investigated. The energy and governing equations were solved by employing the ANSYS Fluent, considering the two-dimensional flow, heat transfer and radiation effects. The influences of core size, shell thickness and material type, PCM mass and shell volume concentrations as the key factors affecting the slurry's photothermal conversion performance in the heat storage medium were analysed. It was found that the nanoencapsulated PCM slurry enhanced the solar system's thermal performance thus storage capacity. The heat transfer rates of water-based Ag, Au, Cu and Al nanofluids were 6.89, 5.86, 7.05 and 6.99 W, respectively. With the addition of Paraffin@Ag, Au, Cu and Al nanocapsules to pure water, the enhancement in heat transfer achieved as 6.18, 13.38, 10.8 and 11.33 %, respectively. Besides, augmenting the nano capsule size depending on the core and shell thickness caused a diminish in the *SA:V* at constant volume concentration, allowed the nano capsules to aggregate at the base fluid. This reduced the heat and energy storage gains of the slurry. As the particle diameter of Paraffin@Ag, Au, Cu and Al composite PCMs enhanced from 18 to 48 nm at PCM mass concentration of 5 %, the heat energy ratios diminished by 5.3, 15.9, 5.15, and 5 %, respectively.

It was also found that improving the PCM mass concentration from 5 to 20 % enhanced the energy gain of the heat storage medium. The thermal energy storage enhancement was calculated as 13.1, 22.5, 18.75, and 20.4 %, respectively as the PCM concentration augmented to the 20 % at the constant particle size of 20 nm. Further, various types of shell materials had different effects on the photothermal conversion performance due to their different thermophysical and optical behaviours. For example, when the shell volume concentration was 10 ppm, the heat energy ratios that paraffin@Ag, Al, Au, and Cu slurries could store relative to pure water were 3.65, 3.23, 3.64 and 3.7, respectively. In addition, although the enhancement in the shell volume concentration increased the temperature increment of the nanoencapsulated PCM slurry, it was noticed that it diminished the system's overall performance by augmenting the heat losses from the collector to the atmosphere. For instance, the energy storage augmentation of paraffin@Ag, Al, Au, and Cu composite PCM based slurries diminished by 11.11, 6.82, 7.41, and 7.27 %, respectively when the shell particle concentration improved from 4 to 600 ppm. It was also observed that paraffin/*Al* slurry had the lowest thermal capacity due to the low thermal conductivity and optical behaviour of the *Al* particles. Last but not least, the experimental findings signified that although the PCM's temperature was augmented by enhanced solar heat flux due to improved temperature gain in the liquid phase as a result of higher solar density, it diminished as wind speed increased due to the high heat losses from the storage cavity to the environment because of the forced convection currents.

Consequently, in the directly heated solar system using such a working fluid containing PCM, the solar radiation absorption capacity was improved by the metallic shell materials. This heat transfer fluid with advanced photothermal conversion characteristics, thus, can be used in future applications for solar energy systems, as it can be used both as a storage and working fluid.

CRediT authorship contribution statement

Oguzhan Kazaz: Conceptualization, Data curation, Formal analysis, Investigation, Methodology, Software, Validation, Visualization, Writing – original draft. **Nader Karimi:** Supervision, Writing – review & editing, Conceptualization. **Shanmugam Kumar:** Supervision, Writing – review & editing. **Gioia Falcone:** Supervision, Writing – review & editing. **Manosh C. Paul:** Conceptualization, Funding acquisition, Project administration, Resources, Supervision, Writing – review & editing.

Declaration of competing interest

The authors declare that they have no known competing financial interests or personal relationships that could have appeared to influence the work reported in this paper.

Data availability

Data will be made available on request.

Acknowledgments

The first author would like to thank the Turkish Ministry of National Education, Republic of Turkey for funding his PhD research study at the University of Glasgow. MCP also acknowledges Engineering and Physical Sciences Research Council (EPSRC) [EP/X027783/1, EP/T022701/1].

References

[1] O. Kazaz, R. Ferraro, M. Tassieri, S. Kumar, G. Falcone, N. Karimi, M.C. Paul, Sensible heat thermal energy storage performance of mono and blended nanofluids in a free convective-radiation inclined system, Case Stud. Therm. Eng. 51 (2023) 103562.
[2] S. Sikiru, T.L. Oladosu, T.I. Amosa, S.Y. Kolawole, H. Soleimani, Recent advances and impact of phase change materials on solar energy: a comprehensive review, J. Energy Storage 53 (2022) 105200.
[3] L. Xing, Y. Ha, R. Wang, Z. Li, Recent advances of solar thermal conversion with wide absorption spectrum based on plasmonic nanofluids, Sol. Energy 262 (2023) 111858.
[4] B. Liu, X. Zhang, J. Ji, Review on solar collector systems integrated with phase-change material thermal storage technology and their residential applications, Int. J. Energy Res. 45 (6) (2021) 8347–8369.
[5] A. Mourad, A. Aissa, Z. Said, O. Younis, M. Iqbal, A. Alazzam, Recent advances on the applications of phase change materials for solar collectors, practical limitations, and challenges: a critical review, J. Energy Storage 49 (2022) 104186.
[6] H. Teamah, M. Teamah, Integration of phase change material in flat plate solar water collector: a state of the art, opportunities, and challenges, J. Energy Storage 54 (2022) 105357.
[7] A. Bejan, C. Teodosiu, C.V. Croitoru, T. Catalina, I. Nastase, Experimental investigation of transpired solar collectors with/without phase change materials, Sol. Energy 214 (2021) 478–490.
[8] L. Feng, J. Liu, H. Lu, Y. Chen, S. Wu, A parametric study on the efficiency of a solar evacuated tube collector using phase change materials: a transient simulation, Renew. Energy 199 (2022) 745–758.
[9] M. Palacio, A. Rincón, M. Carmona, Experimental comparative analysis of a flat plate solar collector with and without PCM, Sol. Energy 206 (2020) 708–721.
[10] Y. Sheikh, M.O. Hamdan, S. Sakhi, A review on micro-encapsulated phase change materials (EPCM) used for thermal management and energy storage systems: fundamentals, materials, synthesis and applications, J. Energy Storage 72 (Part C) (2023) 108472.
[11] A. Palacios, M.E. Navarro-Rivero, B. Zou, Z. Jiang, M.T. Harrison, Y. Ding, A perspective on phase change material encapsulation: guidance for encapsulation design methodology from low to high-temperature thermal energy storage applications, J. Energy Storage 72 (Part E) (2023) 108597.
[12] S. Basriati, H. Saleh, Mathematical modeling of unsteady convective flow analysis of water and nano-encapsulated phase change particles in composite enclosure subject to rotation, J. Energy Storage 72 (Part C) (2023) 108393.
[13] K. Dutkowski, K. Marcin, M. Kochanowska, Experimental studies of the pressure drop in the flow of a microencapsulated phase-change material slurry in the range of the critical Reynolds number, Energies 16 (19) (2023) 6926.

[14] M.K. Yeşilyurt, Ö. Çomakli, Encapsulated phase change material slurries as working fluid in novel photovoltaic thermal liquid systems: a comprehensive review, Iran. J. Sci. Technol. - Trans. Mech. Eng. 47 (2023) 1275–1305.
[15] S.S. Ayyaril, A. Shanableh, S. Bhattacharjee, M. Rawas-Qalaji, R. Cagliani, A. G. Shabib, M. Imran Khan, Recent progress in micro and nano-encapsulation techniques for environmental applications: a review, Results Eng. 18 (2023) 101094.
[16] M. Eisapour, A.H. Eisapour, M.J. Hosseini, P. Talebizadehsardari, Exergy and energy analysis of wavy tubes photovoltaic-thermal systems using microencapsulated PCM nano-slurry coolant fluid, Appl. Energy 266 (2020) 114849.
[17] Y. Jia, C. Zhu, G. Fang, Performance optimization of a photovoltaic/thermal collector using microencapsulated phase change slurry, Int. J. Energy Res. 44 (3) (2020) 1812–1827.
[18] Z. Qiu, X. Zhao, P. Li, X. Zhang, S. Ali, J. Tan, Theoretical investigation of the energy performance of a novel MPCM (microencapsulated phase change material) slurry based PV/T module, Energy 87 (2015) 686–698.
[19] O. Kazaz, N. Karimi, S. Kumar, G. Falcone, M.C. Paul, Investigation of nanoparticle effect in phase change material balls for solar energy conversion and storage systems, in: 15th International Green Energy Conference (IGEC-XV), Glasgow, UK, 2023.
[20] O. Kazaz, N. Karimi, S. Kumar, G. Falcone, M.C. Paul, Nanoencapsulation of phase change materials with metallic shell materials for solar thermal energy harvesting and conversion applications, in: 2nd World Energy Conference and 7th UK Energy Storage Conference, Birmingham, United Kingdom, 2022.
[21] Z. Liu, Z. Chen, F. Yu, Enhanced thermal conductivity of microencapsulated phase change materials based on graphene oxide and carbon nanotube hybrid filler, Sol. Energy Mater. Sol. Cells 192 (2019) 72–80.
[22] X. Ma, Y. Liu, H. Liu, L. Zhang, B. Xu, F. Xiao, Fabrication of novel slurry containing graphene oxide-modified microencapsulated phase change material for direct absorption solar collector, Sol. Energy Mater. Sol. Cells 188 (2018) 73–80.
[23] B. Xu, C. Chen, J. Zhou, Z. Ni, X. Ma, Preparation of novel microencapsulated phase change material with Cu-Cu2O/CNTs as the shell and their dispersed slurry for direct absorption solar collectors, Sol. Energy Mater. Sol. Cells 200 (2019) 109980.
[24] C. Liu, Z. Rao, J. Zhao, Y. Huo, Y. Li, Review on nanoencapsulated phase change materials: preparation, characterization and heat transfer enhancement, Nano Energy 13 (2015) 814–826.
[25] E.M. Shchukina, M. Graham, Z. Zheng, D.G. Shchukin, Nanoencapsulation of phase change materials for advanced thermal energy storage systems, Chem. Soc. Rev. 47 (11) (2018) 4156–4175.
[26] G. Peng, G. Dou, Y. Hu, Y. Sun, Z. Chen, Phase change material (PCM) microcapsules for thermal energy storage, Adv. Polym. Technol. (2020) 1–20.
[27] X. Zhou, S. Yamashita, M. Kubota, H. Kita, Encapsulated copper-based phase-change materials for high-temperature heat storage, ACS Omega 7 (6) (2022) 5442–5452.
[28] B. Zhao, R. Liu, N. Sheng, Y. Mahmoudi, C. Zhu, Copper–alumina capsules for high-temperature thermal energy storage, ACS Appl. Eng. Mater. 1 (5) (2023) 1335–1342.
[29] P. Raj, S. Subudhi, A review of studies using nanofluids in flat-plate and direct absorption solar collectors, Renew. Sust. Energ. Rev. 84 (2018) 54–74.
[30] O. Kazaz, N. Karimi, S. Kumar, G. Falcone, M.C. Paul, Effects of combined radiation and forced convection on a directly capturing solar energy system, Therm. Sci. Eng. Prog. 40 (2023) 101797.
[31] O. Kazaz, N. Karimi, S. Kumar, G. Falcone, M.C. Paul, Heat transfer characteristics of fluids containing paraffin core-metallic shell nanoencapsulated phase change materials for advanced thermal energy conversion and storage applications, J. Mol. Liq. 385 (2023) 122385.
[32] ANSYS Fluent User's Guide, ANSYS, Inc., Canonsburg, 2013.
[33] H. Tyagi, P. Phelan, R. Prasher, Predicted efficiency of a low-temperature Nanofluid-based direct absorption solar collector, J. Sol. Energy Eng. 131 (4) (2009) 041004.
[34] C.F. Bohren, D.R. Huffman, Absorption and Scattering of Light by Small Particles, Wiley, New York, 1983.
[35] W. Lv, P.E. Phelan, R. Swaminathan, T.P. Otanicar, R.A. Taylor, Multifunctional core-shell nanoparticle suspensions for efficient absorption, J. Sol. Energy Eng. 135 (2) (2013) 021004.
[36] A.E. Neeves, M.H. Birnboim, Composite structures for the enhancement of nonlinear-optical susceptibility, J. Opt. Soc. Am. B 6 (4) (1989) 787–796.
[37] Y. Wu, L. Zhou, X. Du, Y. Yang, Optical and thermal radiative properties of plasmonic nanofluids, Int. J. Heat Mass Transf. 82 (2015) 545–554.
[38] H. Duan, R. Chen, Y. Zheng, C. Xu, Photothermal properties of plasmonic nanoshell-blended nanofluid for direct solar thermal absorption, Opt. Express 26 (23) (2018) 29956–29967.
[39] S. Schelm, G.B. Smith, Evaluation of the limits of resonance tunability in metallic nanoshells with a spectral averaging method, J. Opt. Soc. Am. A 22 (7) (2005) 1288–1292.
[40] G.M. Hale, M.R. Querry, Optical constants of water in the 200-nm to 200-μm wavelength region, Appl. Opt. 12 (3) (1973) 555–563.
[41] E.D. Palik, Handbook of Optical Constants of Solids, Academic Press, 1997.
[42] M. Ma, Q. Ai, M. Xie, Optical properties of four types paraffin, Optik 249 (2022) 168277.
[43] S. Babar, J.H. Weaver, Optical constants of Cu, Ag, and Au revisited, Appl. Opt. 54 (3) (2015) 477–481.
[44] M.A. Ordal, L.L. Long, R.J. Bell, S.E. Bell, R.R. Bell, R.W. Alexander, C.A. Ward, Optical properties of the metals Al, Co, Cu, Au, Fe, Pb, Ni, Pd, Pt, Ag, Ti, and W in the infrared and far infrared, Appl. Opt. 22 (7) (1983) 1099–1119.
[45] J.A. Duffie, W.A. Beckman, Solar Engineering of Thermal Processes, John Wiley & Sons, Inc., Hoboken, New Jersey, 2013.
[46] O. Kazaz, N. Karimi, S. Kumar, G. Falcone, M.C. Paul, Enhanced sensible heat storage capacity of nanofluids by improving the photothermal conversion performance with direct radiative absorption of solar energy, J. Mol. Liq. 372 (2023) 121182.
[47] K. Khanafer, K. Vafai, M. Lightstone, Buoyancy-driven heat transfer enhancement in a two-dimensional enclosure utilizing nanofluids, Int. J. Heat Mass Transf. 46 (19) (2003) 3639–3653.
[48] P. Ternik, Conduction and convection heat transfer characteristics of water–Au nanofluid in a cubic enclosure with differentially heated side walls, Int. J. Heat Mass Transf. 80 (2015) 368–375.
[49] O.Z. Sharaf, A.N. Al-Khateeb, D.C. Kyritsis, E. Abu-Nada, Direct absorption solar collector (DASC) modeling and simulation using a novel Eulerian-Lagrangian hybrid approach: optical, thermal, and hydrodynamic interactions, Appl. Energy 231 (2018) 1132–1145.
[50] M. Sheikholeslami, D.D. Ganji, H.R. Ashorynejad, Investigation of squeezing unsteady nanofluid flow using ADM, Powder Technol. 239 (2013) 259–265.
[51] W. Su, J. Darkwa, G. Kokogiannakis, Review of solid–liquid phase change materials and their encapsulation technologies, Renew. Sust. Energ. Rev. 48 (2015) 373–391.
[52] H. Mehling, L.F. Cabeza, Heat and Cold Storage with PCM: An up to Date Introduction Into Basics and Applications, 2008.
[53] T. Bohdal, K. Dutkowski, M. Kruzel, Experimental studies of the effect of microencapsulated PCM slurry on the efficiency of a liquid solar collector, Materials 15 (13) (2022) 4493.
[54] R.R. Kumar, M. Samykano, A.K. Pandey, K. Kadirgama, V.V. Tyagi, Phase change materials and nano-enhanced phase change materials for thermal energy storage in photovoltaic thermal systems: a futuristic approach and its technical challenges, Renew. Sust. Energ. Rev. 133 (2020) 110341.
[55] S. Kumar, A. Kumar, N. Chander, D.K. Singh, Thermal performance analysis of a novel direct absorption solar collector augmented solar still using silver nanofluids, Environ. Prog. Sustain. Energy 41 (5) (2022) e13858.
[56] B.V. Balakin, M. Stava, A. Kosinska, Photothermal convection of a magnetic nanofluid in a direct absorption solar collector, Sol. Energy 239 (2022) 33–39.
[57] "https://www.rubitherm.eu/en/," Rubitherm Technologies GmbH. [Online]. [Accessed 2023].
[58] M. Hosseini, A.A. Ranjbar, K. Sedighi, M. Rahimi, A combined experimental and computational study on the melting behavior of a medium temperature phase change storage material inside shell and tube heat exchanger, Int. Commun. Heat Mass Transf. 39 (9) (2012) 1416–1424.
[59] G.S. Sodhi, K. Vigneshwaran, P. Muthukumar, Experimental investigations of high-temperature shell and multi-tube latent heat storage system, Appl. Therm. Eng. 198 (2021) 117491.
[60] I.A. Siyabi, S. Khanna, T. Mallick, S. Sundaram, Experimental and numerical study on the effect of multiple phase change materials thermal energy storage system, J. Energy Storage 36 (2021) 102226.
[61] X. Liu, Z. Zhang, C. Zhu, F. Wang, D. Zhao, Z. Li, Y. Liu, H. Zhang, H. Jiang, Experimental investigation on the effect of phase change materials for thermal management improvement of the fast charging power module, Case Stud. Therm. Eng. 42 (2023) 102711.
[62] S. Khanna, K.S. Reddy, T.K. Mallick, Performance analysis of tilted photovoltaic system integrated with phase change material under varying operating conditions, Energy 133 (2017) 887–899.
[63] B. Kamkari, H.J. Amlashi, Numerical simulation and experimental verification of constrained melting of phase change material in inclined rectangular enclosures, Int. Commun. Heat Mass Transf. 88 (2017) 211–219.
[64] G.S. Sodhi, P. Muthukumar, Compound charging and discharging enhancement in multi-PCM system using non-uniform fin distribution, Renew. Energy 171 (2021) 299–314.
[65] Y. Tao, Y.K. Liu, Y.-L. He, Effects of PCM arrangement and natural convection on charging and discharging performance of shell-and-tube LHS unit, Int. J. Heat Mass Transf. 115 (Part B) (2017) 99–107.
[66] A. Fragnito, N. Bianco, M. Iasiello, G.M. Mauro, L. Mongibello, Experimental and numerical analysis of a phase change material-based shell-and-tube heat exchanger for cold thermal energy storage, J. Energy Storage 56 (Part A) (2022) 105975.
[67] M. Goel, S.K. Roy, S. Sengupta, Laminar forced convection heat transfer in microcapsulated phase change material suspensions, Int. J. Heat Mass Transf. 37 (4) (1994) 593–604.
[68] B.J. Lee, K. Park, T. Walsh, L. Xu, Radiative heat transfer analysis in plasmonic nanofluids for direct solar thermal absorption, J. Sol. Energy Eng. 134 (2) (2012) 021009.
[69] H. Nikpourian, A.R. Bahramian, M. Abdollahi, On the thermal performance of a novel PCM nanocapsule: the effect of core/shell, Renew. Energy 151 (2020) 322–331.
[70] X. Hu, Z. Huang, Y. Zhang, Preparation of CMC-modified melamine resin spherical nano-phase change energy storage materials, Carbohydr. Polym. 101 (2014) 83–88.
[71] G. Qiao, M. Lasfargues, A. Alexiadis, Y. Ding, Simulation and experimental study of the specific heat capacity of molten salt based nanofluids, Appl. Therm. Eng. 111 (2017) 1517–1522.

[72] Z. Rao, S. Wang, F. Peng, Molecular dynamics simulations of nano-encapsulated and nanoparticle-enhanced thermal energy storage phase change materials, Int. J. Heat Mass Transf. 66 (2013) 575–584.
[73] H. Duan, L. Tang, Y. Zheng, C. Xu, Effect of plasmonic nanoshell-based nanofluid on efficiency of direct solar, Appl. Therm. Eng. 133 (2018) 188–193.
[74] E.M. Languri, H.B. Rokni, Flow of microencapsulated phase change material slurry through planar spiral coil, Heat Transfer Eng. 39 (11) (2018) 977–984.
[75] M.A. Ashraf, W. Peng, Y. Zare, K.Y. Rhee, Effects of size and aggregation/agglomeration of nanoparticles on the interfacial/interphase properties and tensile strength of polymer nanocomposites, Nanoscale Res. Lett. 13 (214) (2018) 1–7.
[76] V. Bhalla, H. Tyagi, Parameters influencing the performance of nanoparticles-laden fluid-based solar thermal collectors: a review on optical properties, Renew. Sust. Energ. Rev. 84 (2018) 12–42.